TITLE

Precise generation of bystander-free mouse models with ABE9-SpRY.

AUTHORS

Jun Kai Ong[1,6], Sayari Bhunia[1,2,3], Beate Hilbert[1], Vanessa Kirschner[1,2], Sascha Duglosz[4], Frank Zimmermann[4], Marc Freichel[1,2] *, Alex Cornean[1,2,5] *

[1] Institute of Pharmacology, Heidelberg University, Heidelberg, 69120, Germany
[2] DZHK (German Center for Cardiovascular Research), Partner Site Heidelberg/Mannheim, Heidelberg University, Heidelberg, 69120, Germany
[3] Heidelberg Biosciences International Graduate School (HBIGS), Heidelberg, 69120, Germany
[4] Interfacultary Biomedical Faculty (IBF), Heidelberg University, Heidelberg, 69120, Germany
[5] DataHarmony Ltd, Milborne Port, Somerset, DT9 5FN, United Kingdom
[6] Present Address: Medizinische Klinik II, Uniklinikum Würzburg, Würzburg, 97078, Germany

* To whom correspondence should be addressed.
Email: alex.cornean@pharma.uni-heidelberg.de.
Correspondence may also be addressed to marc.freichel@pharma.uni-heidelberg.de.

Keywords: adenine base editing, precision editing, mouse modelling, CRISPR/Cas9, hiPS cells

ABSTRACT

Point mutations cause many genetic disorders, but modelling them in organisms is technically challenging. Creating mouse models that mimic these mutations is crucial for establishing a causal relationship between mutations and disease phenotype, thereby supporting the development of therapeutic strategies. Adenine base editors (ABEs) can correct single-nucleotide variants (SNVs) in disease modelling without double-stranded breaks (DSBs) or donor DNA, achieving higher product purity than traditional Cas9 methods. Earlier ABE techniques faced issues like limited targetability, bystander editing, and off-target effects. By combining two editor advancements, we introduced and tested ABE9-SpRY, an improved ABE variant fused with a PAM-flexible SpRY-Cas9 nickase. Our results show that ABE9-SpRY effectively generates three out of four targeted A-to-G mutations in mouse embryos, with significantly fewer off-target effects than ABE8e-SpRY, achieving desired editing efficiencies of up to 96% in individual adult founder mice. ABE9-SpRY also enhances product purity in mouse embryos and human induced pluripotent stem cells (hiPSCs) compared to ABE8e-SpRY. Our findings showcase ABE9-SpRY's precision and versatility, highlighting it as a powerful tool for accurate *in vivo* point mutation modelling.

INTRODUCTION

Disease models have been indispensable in advancing biomedical research by enabling the study of complex physiological and biological interactions that are difficult to replicate *in vitro* (1). The mouse has emerged as the dominating biomedical model due to its genetic, biological, and behavioural similarities to humans, along with the availability of advanced genetic tools for manipulation (2). Moreover, mouse models with disease-relevant mutations or mutations in a given drug receptor have tremendous value for the development and validation of the mode of action of new therapies (3-5). In parallel, hiPSCs have also become a powerful *in vitro* model, providing a human-specific system for studying disease mechanisms, drug responses, and genetic modifications in a physiologically relevant context (6).

The recent development of precise CRISPR/Cas-based gene editing tools has significantly expanded the possibilities for creating genetically engineered mouse models. Notably, the CRISPR/Cas9 system has enabled precise gene modifications by inducing DSBs at specific genomic loci (7). Its efficiency, widespread adaptation and simplicity have made CRISPR/Cas9 the most widely used system for gene editing. However, the CRISPR/Cas9 system has its limitations. The requirement for DSBs introduces risks such as off-target effects and the formation of insertions or deletions (indels) due to the predominant non-homologous end-joining (NHEJ) repair pathway, which can unintentionally disrupt the targeted site or introduce unintended mutations elsewhere (8,9). Likewise, larger deletions (10) and chromosomal aberrations (11) have been reported to occur at significantly higher frequencies with DSB-inducing genome editing approaches.

To address the limitations of DSBs, DNA base editing has emerged, which is catalysed by a new class of tools known as base editors (12,13). Base editors allow single nucleotide conversions without needing DSBs or donor DNA templates. ABEs are of particular interest for introducing A-to-G (or T-to-C) base transitions (12), which are relevant to a wide range of genetic disorders. For example, G•C to A•T mutations account for approximately 47% of the most common pathogenic SNPs in the ClinVar database (14). By fusing a Cas9 nickase (Cas9n) with a deaminase enzyme that converts adenine to inosine, then read as guanine by the cell, ABEs have been used to install point mutations with high efficiency and precision (12,15).

ABEs, therefore, hold immense promise for enabling the rapid and precise generation of disease models in animal and cell models, especially in mice. However, current ABE approaches in mice are limited by bystander editing, issues of targetability and off-target (OT) editing **(Figure 1**). Bystander editing occurs when nucleotides within the editing window of the deaminase, other than the target site(s), are also edited (14), leading to unwanted mutations and making it difficult to study the disease mutations specifically. Canonical ABEs are also limited by their dependency on the NGG protospacer adjacent motif (PAM) recognised by the commonly used *Streptococcus pyogenes* Cas9 (*Sp*Cas9) nickase,

restricting the range of targetable sites in the genome (12). Both Cas-dependent, guided by the sgRNAs' base pairing properties to similar genomic regions (16,17), and Cas9-independent off-target editing, based on deaminase activity on adenines in single-stranded DNA regions outside the targeted site (18,19), have raised serious concerns. These limitations have driven efforts to improve ABEs through directed evolution and rational design. Next-generation variants, such as ABE8e (20), exhibit enhanced deaminase activity, whereas ABE9 has increased specificity due to a narrower editing window (21). Additionally, engineered Cas9 variants like SpRY, which have relaxed PAM requirements, have expanded the range of targetable sequences, allowing for more flexible editing across the genome (22). We therefore aimed to combine the specificity of the ABE9 deaminase with the flexibility of SpRY, thereby overcoming all three challenges and benchmarking these against ABE8e-SpRY (23), to establish four different mouse models with precise point mutations in the ion channels TPC1, TPC2, and TRPM4. These channels play critical roles in physiological processes, and mutations in these channels have been linked to diseases, particularly affecting hepatic and cardiovascular tissues (24-28).

To streamline the generation of disease models in mice and substantially reduce the number of required animals, we established a workflow to characterise and employ ABE9-SpRY for the rapid introduction of desired mutations. After initial benchmarking and strategy design, we cloned and tested the desired sgRNA/ABE-SpRY combinations in N2a cells, followed by pooled injection of synthetic sgRNAs and SpRY-ABEs mRNA into mouse zygotes and analysis of all target and selected OT sites in E14 embryos. Our strategy enabled generating two point mutation mouse models in the absence of bystander editing and with high efficiency for *Tpc1*^{I486T} and *Trpm4*^{L903P}, which can, due to its broad targetability, be used to create a substantial fraction of A-to-G-based mouse models.

RESULTS

Efficient and precise A-to-G base editing with ABE9 in human cells

The most widely used ABE variant today is ABE8e, recognised for its high deaminase activity and processivity (20). However, the increased catalytic activity coincides with a significant broadening of the editing window, expanding from adenine positions A4-A8 in ABEmax to A3-A10 in ABE8e (29), as well as higher levels of off-target DNA and RNA editing (20,21,29). Therefore, this rise in unwanted on-target bystander and off-target editing raises concerns regarding the safety of ABE8e for potential clinical applications (29). To address these safety concerns, several approaches have frequently been employed in the past (**Table 1**): introducing structure-guided or evolved mutations in the deaminase domain (15,20,21,29-33), splitting the editor (34,35), using low mismatch tolerance Cas variants (36), and fusing the ABE with an effector domain (37).

Among all these options, ABE9, which was derived from ABE8e by introducing two point mutations N108Q and L145T in the deaminase domain, appeared to be the most suitable due to its narrowest editing window to date, located between protospacer positions 5-6, and its strong properties for reducing off-target effects in DNA and RNA (21). To this end, we compared ABE8e and ABE9 at four previously reported ABE target sites in HEK293T cells to confirm their properties (**Supplementary Fig. 1**). Indeed, the editing window of ABE9 was specific to positions A5 and A6, with some minimal activity at A4, whereas ABE8e was highly active between A3 and A8 with an extended activity shoulder to A13. Overall, the average activity at A5 was reduced from 43.6 ± 5.9% (mean±s.d.%) in ABE8e to 34.5 ± 8.8% in ABE9, corresponding to an average reduction of 21% in editing activity, in line with previous work (21) (**Supplementary Fig. 1**). We were, therefore, able to confirm the potential of ABE9 and, encouraged by this, proceeded to apply its precision to our loci of interest.

ABE9-SpRY is a precise and versatile editor in mouse cells

We first designed the sgRNAs for the four loci to position the target adenines within the optimal editing windows of the deaminases of ABE8e and ABE9, respectively (**Figure 2A**). However, the canonical architectures of PAM-interacting motifs in both ABEs, when fused to the standard *Sp*Cas9n, proved unsuitable due to the lack of the NGG PAM sequence.

To address this limitation, we next considered alternative Cas9 variants that have different or relaxed PAM requirements, including *Sa*Cas9, xCas9, *Sp*Cas9-NG, *Sp*Cas9-VQR, and SpRY (22,38-43). Instead of an "on-demand" context-dependent approach, we developed a versatile editing strategy that can be applied to all four loci of interest by utilising a single construct and the appropriate sgRNAs. SpRY (22) and SpRYc (44) have emerged as potentially universal Cas9 variants with PAMless targetability across NNN PAMs (**Table 1**). SpRY stands out for having the broadest and most relaxed

PAM compatibility and has previously been tested with ABE8e variants (31-33). We fused a SpRY nickase (in the following simply "SpRY", bears these substitutions compared to *Sp*Cas9 nickase: A61R/L1111R/D1135L/S1136W/G1218K/E1219Q/N1317R/A1322R/R1333P/R1335Q/T1337R) to the TadA domains of ABE8e or ABE9 to streamline the experimental workflow and maximise the potential for successful genome editing outcomes (**Figure 2B**). These SpRY base editors can, in theory, effectively target spacers with NRN (G or A) PAMs, and to a lesser degree, NYN (T or C) PAMs (22).

Since the compatibility of deaminase domains with Cas9 variants is not universal, and their efficiency and editing activity can vary based on the specific Cas9 variants used (15,45,46), an initial evaluation was necessary. Due to the lack of published reports on ABE9-SpRY, we compared it to ABE8e-SpRY using a plasmid-based lipofection approach alongside the respective sgRNAs for the four loci of interest in mouse Neuro-2a (N2a) cells (**Figure 2C**).

Deep sequencing of transfected cells revealed that the desired editing occurred at all four targets for ABE8e-SpRY, ranging from 14.1 ± 0.7% to 60.6 ± 1.2%. In contrast, only three targets showed targeted A-to-G editing with ABE9-SpRY, ranging from 6.5 ± 0.9% to 13.2 ± 1.5% across all tested sites (**Figure 2D**). While ABE8e-SpRY displayed modest editing of 14.1 ± 0.7% at the *Tpc2-K188* locus, no desired editing was noted with ABE9-SpRY. A closer examination of editing at adenines within the sgRNA target sites confirmed the previously observed broad activity window of ABE8e-SpRY, which included 13.5 ± 0.5% editing at A2 and 20.8 ± 0.6% editing at A12 at the *Tpc1-I486* locus (**Figure 2E**). The highest ABE8e-SpRY activities were observed at A5 (*Tpc2-K188*, *Tpc2-L249*, *Trpm4-L903*) and A6 (*Tpc1-I486)*, with 30.8 ± 0.5%, 26.1 ± 6.5%, 41.9 ± 12.8%, and 61.6 ± 12.7% A-to-G editing, respectively. By contrast, ABE9-SpRY demonstrated the enhanced precision previously observed for ABE9, with the activity window spanning from A4 to A9 at the *Tpc1-I486* locus, showing 9.1 ± 1.3% and 3.3 ± 0.5% editing, respectively. We also measured the highest efficiencies for ABE9-SpRY at A5 and A6, respectively, with 6.5 ± 0.9%, 12.8 ± 0.8%, and 13.7 ± 1.7% efficiency for *Tpc2-L249*, *Trpm4-L903*, and *Tpc1-I486,* respectively. This narrower editing window of ABE9-SpRY also led to a larger fraction of edited alleles containing no bystander mutations compared to ABE8e-SpRY (**Figure 2F**), as indicated by the substantially higher product purity, ranging from 50.9 ± 2.4% to 98.6 ± 0.6%, compared to 1.1 ± 0.1% to 69 ± 0.8% for ABE8e-SpRY (**Figure 2G**). Notably, the desired *Tpc1*^{I486T} and *Trpm4*^{L903P} mutations could not be introduced without bystanders using ABE8e-SpRY (0.7 ± 0.1% and 0.5 ± 0.3%), whereas ABE9-SpRY achieved 6.7 ± 0.4% and 11.9 ± 1.4% precise editing at these sites, respectively. Lastly, ABE9-SpRY demonstrated reduced indel frequencies compared to ABE8e-SpRY across all four sites, peaking at 0.9 ± 0.2% (*Tpc1-I486*) (**Figure 2H**).

Taken together, these *in vitro* results for ABE target sites in mouse cell line indicated that ABE9-SpRY can precisely edit three out of four desired target sites, two of which could not be generated with ABE8e-

159 SpRY due to bystander mutations. Therefore, we next decided to apply these approaches *in vivo*, testing
160 editing efficiencies in mouse embryos.

161 **Multiplexed, precise ABE9-SpRY mouse embryo editing**

162 Adenine base editing in mouse zygotes has been successfully performed using a combination of ABE
163 mRNA and either *in vitro* transcribed or chemically synthesised modified sgRNAs, injected into the
164 cytoplasm or pronucleus of the zygote (37,47-52). Indeed, these efforts have been highly efficient in
165 achieving nearly 100% editing using ABE7.10 (47-49). However, precision issues were apparent, as
166 only 1.3% to 20% of desired edits occurred within an overall A-to-G efficiency of 95% in the
167 protospacer (48).

168 To evaluate the *in vivo* editing efficiency of our approach in mouse embryos, we microinjected a pool
169 of four synthetic sgRNAs along with either *in vitro* transcribed ABE8e-SpRY or ABE9-SpRY mRNA
170 into the cytoplasm of mouse zygotes. The injected zygotes were transferred to pseudopregnant surrogate
171 mothers, isolated on embryonic day 14, and their genomic DNA was extracted for targeted deep
172 sequencing analysis (**Figure 3A**).

173 Our analysis indicated that ABE8e-SpRY effectively edited target adenines at all four sites, achieving
174 editing efficiencies of up to 100%. The average editing efficiencies were 78.9 ± 25.7% at *Tpc1-I486*
175 [median (IQR), 91.4% (67.0-99.9%)], 52.6 ± 30.8% at *Tpc2-K188* [median (IQR), 54.5% (32.9-70.1%)],
176 84.5 ± 20.2% at *Tpc2-L249* [median (IQR), 94.1% (75.1-99.9%)], and 99.8 ± 0.6% at *Trpm4-L903*
177 [median (IQR), 99.9% (41.7-100.0%)], (**Figure 3B**). Editing by ABE9-SpRY was observed at *Tpc1-*
178 *I486T*, *Tpc2-L249*, and *Trpm4-L903P*, achieving efficiencies of up to 59.1%, 62.3%, and 89.3%, with
179 corresponding averages of 11.0 ± 18.1% [median (IQR), 0.04% (0.02-20.26%)], 11.9 ± 16.8% [median
180 (IQR), 6.71% (0.04-12.95%)], and 23.7 ± 28.6% [median (IQR), 8.50% (0.03-48%)], respectively.

181 A closer examination of adenine base editing across the protospacer sequences revealed a pattern
182 consistent with previous *in vitro* findings. Despite the high editing efficiency of ABE8e-SpRY, its
183 activity was broadly distributed, targeting adenines from positions A2 to A14 across all tested loci
184 (**Figure 3C**). In contrast, ABE9-SpRY exhibited a narrower editing window, concentrating edits
185 primarily within positions A4 to A8. Notably, low-level editing was detected in a single embryo at the
186 *Tpc2-K188* locus, where ABE9-SpRY had shown no *in vitro* activity. This editing occurred at only one
187 of the two targeted adenines, resulting in a 25.2% conversion that introduced a p.K188E substitution
188 instead of the intended p.K188G mutation.

189 ABE9-SpRY exhibited a higher rate of desired edits with no bystander edits at the *Tpc1-I486* locus
190 (10.7 ± 17.5% vs 0.3 ± 1.2%) and at *Trpm4-L903* (21.3 ± 28.4% vs 0.0 ± 0.0%). In contrast, ABE8e-
191 SpRY showed more specific activity at *Tpc2-K188* (25.5 ± 25.9% vs 0.0%) and *Tpc2-L249* (52.8 ± 27.5%

192 vs 11.8 ± 16.2%) (**Figure 3D**). Analysing product purity as a measure of precision revealed that ABE9-
193 SpRY generated significantly purer editing outcomes across all active loci: *Tpc1-I486* (85.1 ± 30.6%
194 vs 1.2 ± 5.3%), *Tpc2-L249* (94.6 ± 22.3% vs 60.8 ± 27.1%), and *Trpm4-L903* (90.5 ± 20.8% vs 0.0%)
195 (**Figure 3E**). Furthermore, ABE9-SpRY produced only low levels of indels, similar to ABE8e-SpRY
196 (**Figure 3F**).

197 Only one C-to-T conversion was noted at the *Tpc1-I486* locus in an embryo edited with ABE8e-SpRY,
198 occurring at a frequency of 12.6% at position C6, alongside a single instance of 34.7% unwanted A-to-
199 C editing (**Supplementary Fig. 2A**). Additionally, an unexpected off-target modification was found
200 upstream of the sgRNA binding region at position A-2 of the *Tpc2-L249* locus
201 (**Supplementary Fig. 2B**). This edit appeared in one ABE9-SpRY and one ABE8e-SpRY injected
202 embryo at frequencies of 12.3% and 21.9%, respectively. A possible explanation is the dynamic nature
203 of the Cas9-sgRNA-DNA complex and conformational changes during editing, which may briefly
204 expose adjacent bases to the deaminase domain, leading to unintended deamination events.

205 These findings suggest that ABE9-SpRY provides enhanced editing purity, though it does so at the
206 expense of locus-dependent activity. To further assess precision beyond these target loci, we next
207 analysed both Cas9-dependent and Cas9-independent off-target editing to more thoroughly characterise
208 the safety profiles of these two editors.

209 **ABE9-SpRY substantially decreases off-target effects compared to ABE8e-SpRY**

210 Cas-dependent off-target events arise from the tolerance of mismatches between sgRNA and the
211 targeting sequence. Although SpRY can target a broader range of genomic sites, its relaxed PAM
212 tolerance also implies that the potential Cas-dependent off-target sites are substantially expanded, as
213 sgRNA-DNA mismatches become the sole determinant of off-target binding without PAM constraints.
214 Consequently, we identified the top five predicted off-target sites for each locus using ACEofBASEs
215 (53) and analysed these sites across three embryos per group.

216 When analysing the cumulative percentage of reads containing edits in the off-target spacer sequences,
217 we found that the average cumulative A-to-G editing in the off-target protospacer at the *Tpc1-I486* off-
218 target sites varied from 4.1 ± 5.7% to 264.3 ± 15.6% for ABE8e-SpRY, compared to baseline control
219 levels for ABE9-SpRY (**Figure 4A, Supplementary Figure 3**). Off-target editing at the highest edited
220 adenines ranged from 4.1 ± 7.0% at OT2 to 27.8 ± 17.4% at OT3 for ABE8e-SpRY
221 (**Supplementary Figure 3**). Overall, across 20 off-target sites with various PAM sequences, ABE8e-
222 SpRY induced A-to-G edits above control levels at 14 sites, especially at protospacer positions A2 to
223 A20 (**Figure 4A–D, Supplementary Figures 3–6**). In contrast, ABE9-SpRY edited just two off-target
224 sites associated with the *Tpc2-L249* locus, reaching 40.0% and 48.1% editing, respectively (**Figure 4C,
225 Supplementary Figure 5**). Strikingly, for these two off-target sites, the corresponding embryos' on-

226 target editing efficiencies at the locus were relatively low, at 7.4% and 10.7%. While off-target effects
227 are known to occur with base editors, this drastic skew towards off-target editing (with a 3-base
228 mismatch) is remarkable. Since these events were observed in just one replicate of ABE9-SpRY, the
229 data indicate that ABE9-SpRY is a notably improved precision tool, though rare, sequence-dependent
230 off-target activity may still occur.

231 In addition to Cas-dependent off-target effects, base editors have also been reported to exhibit Cas-
232 independent off-target activity, which is evoked by the deaminase activity of the editors (18,19). We
233 therefore asked whether TadA-8e and TadA-9 deaminases cause Cas-independent off-target effects to
234 similar extents, regardless of the Cas9 nickase variant to which they are attached. To this end, we
235 utilised the orthogonal R-loop assay (54) (**Figure 4E**) in HEK293T cells and, after FACS-enrichment
236 of GFP co-transfected cells, observed no editing across eight adenines and three R-loop spacers with
237 ABE9-SpRY, similar to the results reported earlier for ABE9 (21). In contrast, ABE8e-SpRY caused
238 substantial editing from 4.3 ± 1.1% (R loop 1), 7.7 ± 2.7% (R loop 2), to 12.0 ± 1.4% (R loop 3). These
239 results highlight the high specificity of ABE9-SpRY despite the increased non-specific binding of
240 SpRY.

241 **ABE9-SpRY is effective at generating precise *Tpc1*^{I486T} and *Trpm4*^{L903P} founder mice**

242 Accurate base conversion is crucial for modelling SNVs; therefore, minimising bystander and off-target
243 mutations is essential. Given the negligible levels of bystander editing, low Cas9-dependent off-target
244 editing, and no evidence above background of Cas9-independent off-target editing produced by ABE9-
245 SpRY, we decided to use this editor for generating two individual founder mouse lines harbouring the
246 *Tpc1*^{I486T} and *Trpm4*^{L903P} mutations. To achieve this, ABE9-SpRY and the locus-specific sgRNAs were
247 injected separately into mouse zygotes. Analysis of adult mice biopsies from 48 putative F0 founder
248 mice revealed robust editing efficiencies (**Figure 5A-B**), with the precise, bystander, and indel-free
249 p.I486T achieved at 25.6 ± 21.0% efficiency [median (IQR), 26.1% (4.9-44.7%)], and up to 81.4%
250 (**Figure 5B**). The very low rate of bystander editing at A4 (**Figure 5B**) resulted in a considerable
251 product purity of 96.4 ± 13.8% [median (IQR), 98.9% (98.8-99.0%)] (**Figure 5C**). While one individual
252 mouse exhibited an indel frequency of 11.2% at the *Tpc1-I486* locus, overall indel levels were generally
253 minimal (0.3 ± 1.6%). Analysis of 36 *Trpm4-L903* ABE9-SpRY edited mice showed a similar trend
254 (**Figure 5D-E**). The product purity was comparable, as observed for *Tpc1-I486*, at 93.9 ± 10.3%
255 [median (IQR), 97.6% (97.4-97.8%)] (**Figure 5F**), due to the limited bystander editing events at A8
256 (**Figure 5C**). Overall, p.L903P was accurately and precisely established at even higher efficiencies than
257 p.I486T, at frequencies of 28.3 ± 20.8% [median (IQR), 21.2% (10.4-34.7%)], and up to 96.0%
258 (**Figure 5E**). Similarly, indel frequencies were slightly higher at the *Trpm4-L903* locus at 1.0 ± 5.9%,
259 reaching 35.5% in one instance.

To determine the F1 transmission rate and establish stable mutant lines for *Tpc1* p.I486T and *Trpm4* p.L903P, we proceeded to mate two verified adult F0 *Tpc1* p.I486T male mice **(Figure 5B)** and three verified adult F0 *Trpm4* p.L903P male mice **(Figure 5E)** with wild-type females. We observed high transmission rates for *Tpc1* p.I486T of 55.6% and 62.5% in the two independent matings **(Figure 5G, Supplementary Figure 7A)**, and high to complete transmission for *Trpm4* p.L903P at rates ranging from 80% to 100% **(Figure 5H, Supplementary Figure 7B)**. Finally, we mated select heterozygous F1 carriers with wild-type mice to establish stable lines (**Supplementary Figure 8).**

These results suggest that the pooled embryo analysis has somewhat underestimated the potential editing efficiency of ABE9-SpRY when deployed to individual loci rather than diluted across several for screening. Moreover, the highly precise editing rates and encouraging off-target profile indicate the potential for direct founder-generation phenotyping, which could accelerate experimental timelines and reduce both resource consumption and the number of animals required.

Precise hiPSC engineering with ABE9-SpRY

Over the past two decades, hiPSCs have become a powerful *in vitro* model, offering a human-specific system for studying disease mechanisms, drug responses, and genetic variants in a physiologically relevant context when paired with directed-differentiation procedures (55,56). Given this importance, we aimed to validate the potential of ABE9-SpRY for disease modelling in hiPSCs. To enrich base-edited cells, we used the XMAS-TREE assay (57), in which a successful A-to-G conversion of a stop codon in between an episomal mCherry-linker-EGFP construct leads to the co-expression of GFP alongside the pre-existing mCherry signal (**Figure 6A**). We selected the human p.I485T mutation of human *TPC1*, corresponding to mouse *Tpc1* p.I486T, as a test and designed two sgRNAs with the target adenine located either in position A5 (sgRNA#2) or A6 (sgRNA#1) of the protospacer sequence, respectively (**Figure 6B**). We then co-transfected either ABE8e-SpRY or ABE9-SpRY plasmid, which we re-cloned under an EF1α promoter for robust hiPSC expression, along with the reporter plasmid, a reporter-STOP-sgRNA plasmid, and either of the two target sgRNA plasmids, thereby enriching the base-edited cell population through FACS sorting (**Figure 6C**). While the overall editing efficiency was substantially higher with ABE8e-SpRY, 75.8 ± 1.0% editing with sgRNA#1 and 33.7 ± 2.0% with sgRNA#2, ABE8e-SpRY was also active very broadly. In particular, the two adjacent bases A4 and A6, or A3 and A5 for sgRNA#1 and sgRNA#2, respectively, displayed very similar activity. By contrast, ABE9-SpRY achieved efficiencies of only up to 10.9 ± 0.7% (**Figure 6D**). However, we observed superior overall desired editing activity without unwanted mutations, a result of the higher precision, with sgRNA#1 reaching 9.9 ± 0.7%. Notably, despite ideal target site positioning, sgRNA#2 showed a slightly lower efficiency at 7.6 ± 0.6% (**Figure 6E**). The highest editing rate without unwanted mutations for ABE8e-SpRY was 3.0 ± 0.1%. While the overall editing rates of ABE9-SpRY were lower, this limitation is less critical in the context of hiPSC-based disease modelling, where correctly edited

295 clones are typically isolated and expanded prior to downstream differentiation into specific cell types
296 of interest. Importantly, such clonal isolation strategies rely on the high precision of the editing event,
297 which we achieved with ABE9-SpRY, but not ABE8e-SpRY. In addition to the increased frequency of
298 indels observed (**Figure 6F**) at 2.9 ± 0.5% with ABE8e-SpRY compared to 0.1 ± 0.1% with ABE9-
299 SpRY using sgRNA#1, these results further bolster the case for the potential of ABE9-SpRY in a wide
300 variety of precision disease modelling applications, spanning from animal to cellular models.

301 **DISCUSSION**

302 Base editing holds great promise for modelling point mutations due to its benefits over existing
303 techniques, as it prevents DSBs and shows high on-target efficiency (12,13). While previous studies
304 have utilised base editing for animal modelling, they have frequently encountered issues such as off-
305 target effects, bystander editing, and indels (47,48,58,59).

306 Successful disease modelling via base editing requires (1) precise editing with no bystander missense
307 mutations, as they can easily mask or disrupt the interpretation of the desired mutation (60); (2) absence
308 of indels on the same allele to avoid frameshifts and truncated proteins (61); and (3) minimal off-target
309 effects, which, if frequent, can persist despite outcrossing (62) and may necessitate costly genome-wide
310 validation.

311 Here, we utilised the latest advancements in the gene editing toolbox to address these issues. We
312 demonstrated that using ABE9, an adenine base editor recognised for its high specificity and safety
313 profile (21), fused with the PAM-less SpRY-Cas9 nickase (22), can efficiently introduce A-to-G
314 mutations with great flexibility. It results in low to no bystander editing, minimal detectable Cas-
315 dependent off-target effects at only two sites, and very few indels, achieving up to 89% precise editing
316 of desired changes in mouse embryos. Moreover, in adult F0 founder mice, we observed up to 96%
317 desired editing at the *Trpm4-L903* locus, highlighting the potential for phenotyping within the same
318 generation. In contrast, ABE8e-SpRY exhibited a higher overall A-to-G conversion efficiency, close to
319 homozygosity. However, this was accompanied by bystander mutations at similar frequencies, resulting
320 in significantly lower product purities. Furthermore, ABE8e-SpRY caused substantial levels of Cas-
321 dependent off-target editing in mouse embryos at 14 of 20 sites examined, with A-to-G editing
322 frequencies at OT5 of the *Trpm4-L903* sgRNA reaching up to 84%. Therefore, the trade-off between
323 reduced editing efficiency and high precision remains a valuable advantage that ABE9-SpRY offers for
324 generating genetic and disease models where bystander editing is unacceptable.

325 We found that pooling sgRNAs during the initial *in vivo* testing in embryos is an effective strategy. This
326 approach enables rapid screening of editing outcomes with reduced effort and decreases the number of
327 animals required. However, this approach seems to underestimate editing efficiency compared to
328 experiments where only a single sgRNA is injected. For example, at the *Tpc1-I486* locus, perfect editing

329 (desired editing without bystander edits) occurred at a frequency of 10.7 ± 17.5% in embryos (pooled)
330 versus 25.6 ± 21.0% in adults (single). Similarly, at the *Trpm4-L903* locus, the desired editing frequency
331 was 21.3 ± 28.4% (pooled) versus 28.3 ± 20.8% (single). This discrepancy may stem from the dilution
332 of the editing machinery across four different target sites, and potentially their off-targets, in the pooled
333 condition. This likely reduces the effective concentration of the editor at each individual locus, thereby
334 lowering the observed editing efficiency.

335 At the *Tpc2-K188* locus, ABE8e-SpRY demonstrated efficient editing, while only one mouse embryo
336 showed any editing for ABE9-SpRY. This indicates that the SpRY-Cas9n protein can access this target
337 site, but the evolved TadA-9 deaminase enzyme has shown reduced substrate acceptance compared to
338 TadA-8e. Given that the N108Q and L145T mutations in ABE9 are speculated to expel the backbone
339 of the DNA substrate (21), this may also change the substrate-interaction behaviour of TadA-9
340 compared to TadA-8e, in addition to altering the editing window. As such, the observation at the *Tpc2-*
341 *K188* locus suggests that, in addition to altering the editing window, these mutations may create
342 sequence-dependent steric hindrances that prevent the enzyme from effectively engaging with the target
343 adenine, even within its supposedly optimal editing window. To better understand the genome-wide
344 targeting properties of ABE9-SpRY, a combination of detailed structural analyses to elucidate the
345 mechanisms by which the N108Q and L145T mutations influence substrate binding and high-
346 throughput *in vitro* analysis of a large number of disparate target sites will be required. However, despite
347 its efficiency, ABE8e-SpRY would not be the alternative to ABE9-SpRY in cases such as those at the
348 *Tpc2-K188* locus due to its off-target profile. For sites untargetable by ABE9-SpRY, alternative variants
349 with enhanced specificity, such as ABE8e-WA/WQ (30), ABE8e-N108Q (21), ABE8e-V106W (20),
350 and next-generation ABEs (e.g., ABE8r, ABE-Umax, ABEx2/4, E2-/E4-ABE, TadA-8e-L1B_S116,
351 hpABE5.20 (63-68), are emerging and may serve as effective substitutes when fused to SpRY-nickase.
352 In practice, the advent of scalable machine learning-based engineering tools to create bespoke ABE-
353 SpCas9 variants with target-specific PAMs (69) will help to maximise on-target editing by use of the
354 highest activity and precise deaminases with context-specific PAM-interacting motifs, to substantially
355 reduce off-target editing.

356 The PAM-less properties of SpRY, in any combination with next-generation genome editors, present
357 significant challenges of their own, particularly concerning increased off-target genome editing, which
358 consequently leads to a rise in chromosomal rearrangements (11). As a result, ABE-SpRY editors are
359 expected to demonstrate increased off-target editing due to their ability to bind and modify DNA
360 sequences without the stringent necessity for a PAM. ABE8e-SpRY demonstrated extensive Cas9-
361 dependent off-target editing at 70% of the examined off-target sites. At one of these sites, *Trpm4-L903*
362 OT5, editing reached up to 84%. ABE9-SpRY, in contrast, exhibited editing at only 10% of the
363 examined sites. We acknowledge that a limitation of our off-target analysis is its dependence on *in silico*
364 predictions of potential non-specific sgRNA binding sites. This method may introduce bias, as the sites

365 are selected *a priori* and might miss *bona fide* off-target effects. Nonetheless, it remains a common and
366 practical initial method for evaluating base editor specificity. To complement *in silico* predictions, a
367 suite of unbiased genome-wide off-target detection methods has been developed in recent years (70).
368 For adenine base editors, specific unbiased genome assays like EndoV-seq (76), Digenome-seq (77),
369 and Selicit-seq (78) have been developed. Especially when stringent validation is necessary, such as in
370 clinical settings, these should be complemented with detailed chromosome-level structural analyses
371 using assays like CAST-seq (80). Although these advanced methods are valuable, our results using *in*
372 *silico* prediction already demonstrate that ABE9-SpRY strikes an attractive balance of precision and
373 flexibility, supporting its suitability for generating disease models.

374 hiPSCs are increasingly utilised for disease modelling because they closely resemble the human genome
375 and can differentiate into specific tissues (71). As hiPS cell culture continues to advance from traditional
376 2D systems to more intricate 3D models, it enables advanced exploration of pathophysiological
377 mechanisms and disease modelling (72). For this purpose, reproducing genetic variants as precisely as
378 possible is crucial, making the exclusion of bystander editing and limitation of off-target effects
379 indispensable (73). Given the target flexibility of ABE9-SpRY, we designed two tiled sgRNAs across
380 the target site and demonstrated that ABE9-SpRY could precisely induce a single-base change in
381 hiPSCs without bystander editing. Although editing efficiency is relatively low compared to ABE8e-
382 SpRY, and clonal isolation remains necessary for certain downstream gene mutation studies, the
383 absence of bystander editing simplifies the clonal isolation. Utilising reporter assays for editing
384 enrichment, such as XMAS-TREE, and optimising the delivery method will help overcome the
385 limitations of low editing efficiencies (74,75).

386 Overall, ABE9-SpRY demonstrates high precision while maintaining considerable flexibility, which is
387 crucial, as missense mutations can be highly detrimental. For example, in the context of disease rescue,
388 even with ABE8e's high efficiency in introducing the intended point mutation, a bystander edit caused
389 a missense mutation that ultimately prevented phenotypic rescue (60). This underscores the importance
390 of precision editors like ABE9-SpRY, particularly when modelling diseases or designing therapeutic
391 strategies where functional outcomes are paramount. This level of precision is essential for fundamental
392 research, such as structure-function studies of a specific protein domain, where even a single unintended
393 amino acid change introduced by bystander editing could make the results uninterpretable. The potential
394 for base editors to introduce confounding SNVs, as systematically demonstrated in mouse embryos (59),
395 underscores the need for cleaner tools like ABE9-SpRY to produce reliable models for functional
396 analysis. With ABE9-SpRY's versatility in targeting specific adenines, along with minimised bystander
397 editing and reduced Cas-dependent and Cas-independent off-target effects, it represents a valuable tool
398 for creating precise disease models in both animals and cell lines, hiPSCs, and organoids derived from
399 them.

400 **EXPERIMENTAL SECTION**

401 **Reagents and biological resources**

402 Information on major resources is provided in **Supplementary Table 1**.

403 **Mouse strains**

404 Wild-type C57BL/6N mice were purchased from Charles River Laboratories (Wilmington, MA, USA).
405 The experimental procedures were approved by the regional council of Karlsruhe, Germany, in
406 accordance with the Animal Welfare Act (AZ35-9185.81/G-60/23). Microinjection was performed in
407 the cytosol of C57BL/6N zygotes. All animals were housed in the Interfaculty Biomedical Faculty (IBF)
408 of Heidelberg University. Mice were maintained under specified pathogen-free conditions with a 12-
409 hour light/12-hour dark cycle, and water and standard food (Rod18, LASvendi GmbH, Germany)
410 available ad libitum.

411 **Identification and Alignment of Mouse Orthologues for Targeted Point Mutations**

412 To identify the corresponding mutations in the mouse genome, to four target loci of interest with
413 missense mutations *Tpc1 p.I485T*, *Tpc2 p.L265P*, *Tpc2 p.K204A*, and *Trpm4 p.L907P* we retrieved the
414 *Mus musculus* and *Homo sapiens* gene sequences from Ensembl and performed protein sequence
415 alignments. This allowed us to pinpoint the target amino acids and the corresponding adenines in the
416 mouse coding sequence. Through this alignment, we identified the orthologous amino acid residues in
417 the respective mouse genes and the potential missense mutations we can model by A-to-G transition
418 mutation mediated through ABEs: *Tpc1 p.I486T*, *Tpc2 p.L249P*, *Tpc2 p.K188G*, and *Trpm4 p.L903P*.
419 Notably, for *Tpc2 p.K188G*, a glycine substitution was created *in silico* instead of the alanine. We
420 decided to proceed with the glycine substitution based on the similar chemical and functional properties
421 of glycine and alanine.

422 **Design and cloning of sgRNAs**

423 sgRNAs were designed manually to enable the precise installation of the defined missense mutations
424 and validated using ACEofBASEs (53) with the following parameters: select BaseEditor "custom ABE"
425 with Window start "3" and Window end "11" with PAM "NRN" for *Tpc1-I486*, *Tpc2-K188*, and *Trpm4-*
426 *L903* target sites or with PAM "NYN" for the *Tpc2-L249* target site; for Species "Mouse (Mus musculus)
427 Ensembl V 103". The full list of sgRNA oligonucleotides to clone and the sgRNAs used in this study
428 are shown in Supplementary Tables 2 and 3.

429 For *in vitro* applications of sgRNAs, the 20 bp *Sp*Cas9 sgRNA spacer sequences used in this study were
430 designed with the 5' and 3' sequences (**Supplementary Table 2**), as previously described (76), with an
431 additional 5' "G" added in cases in which the spacer does not start with a G. In brief, the 20 bp target

432 site (N20) sequences were ordered as oligonucleotides with the following sequences 5'-CACC(N20-
433 21)GTTTT-3', while the sequences complementary to the target site were designed and ordered as
434 oligonucleotides as follows 5'-CTCTAAAAC(N20-21)-3'. sgRNAs were cloned into the BsaI-digested
435 2.18 kb pU6-pegRNA-GG-acceptor fragment (pU6-pegRNA-GG was a gift from David Liu, Addgene
436 plasmid #132777, (76)) by oligonucleotide annealing and Golden Gate assembly as previously
437 described (76), including the standard *Sp*Cas9 sgRNA scaffold.

438 *R-loop SaCas9 sgRNAs.* To generate the *Sa*Cas9 sgRNA plasmid, BPK1520, containing a
439 pU6_BsmBIcassette-Sp-sgRNA was used as a backbone (BPK1520 was a gift from Keith Joung,
440 Addgene plasmid #65777, (39)). The *Sp*Cas9 sgRNA scaffold was digested using *BsmBI* and *HindIII*,
441 and the digested fragment was isolated. The *Sa*Cas9 sgRNA scaffold sequence (42), designed with
442 complementary overhangs (**Supplementary Table 2**), was ligated into the digested vector backbone.
443 The designed sgRNA spacer sequences were then ordered as oligonucleotides with *BsmBI* overhangs
444 (**Supplementary Table 2**), and the annealed oligos were cloned into the *BsmBI*-digested *Sa*Cas9
445 sgRNA plasmid via Golden Gate assembly. In brief, in a 10 µl reaction volume, 50 ng of *Sa*Cas9 sgRNA
446 plasmid, 10 units of *BsmBI*-v2 (NEB), 20 units of T4 DNA ligase (NEB), 1 µL of 1 µM annealed spacer
447 oligonucleotides, 1X T4 DNA ligase buffer were assembled under the following thermal cycling
448 conditions: digestion at 42°C for 4 minutes, followed by ligation at 16°C for 3 minutes, repeated for a
449 total of 11 cycles. The reaction was then incubated at 80°C for 10 minutes to inactivate *BsmBI*.

450 *hiPSC sgRNAs.* Cloning of targeting sgRNA into the pDT-sgRNA-XMAS-1x plasmid was performed
451 as previously described (pDT-sgRNA-XMAS-1x was a gift from Xiao Wang, Addgene plasmid
452 #164413, was performed as previously described (57)).

453 All sgRNAs for mouse experiments were ordered via Integrated DNA Technologies (IDT) as custom
454 Alt-R CRISPR-Cas9 sgRNA (**Supplementary Table 3**).

455 **Cloning of adenine base editor plasmids**

456 All plasmids constructed here were cloned via Gibson Assembly using the NEBuilder HiFi DNA
457 Assembly (NEB) kit with PCR products amplified from designated template plasmids with specific
458 primers (**Supplementary Table 4**) with Q5 Hot Start DNA polymerase (NEB).

459 To obtain pCMV_ABE9, we used the ABE9 editor sequence form (21), and recloned pCMV_ABE8e
460 (a gift from David Liu, Addgene plasmid #138489, (20)) by introducing the two defining mutations
461 N108Q and L145T by PCR, altogether assembled via four fragments (**Supplementary Table 4**):
462 pCMV_backbone, ABE9_fragment_1_TadA*_Nterm_N108Q,
463 ABE9_fragment_2_TadA*_N108Q_L145T, ABE9_fragment_3_Cas9n-Nterm. To clone
464 pCMV_ABE8e-SpRY, we assembled the following PCR products: pCMV_backbone,

465 ABE8e_fragment1_TadA*, and ABE9-SpRY_fragment_4_SpRY-Cas9n (amplified from pCMV-T7-
466 ABE8e-nSpRY-P2A-EGFP (KAC1069), a gift from Benjamin Kleinstiver, Addgene plasmid #185912,
467 (77)). Similarly, pCMV_ABE9-SpRY was constructed by assembling: pCMV_backbone,
468 ABE9_fragment_1_TadA*_Nterm_N108Q, ABE9_fragment_2_TadA*_N108Q_L145T,
469 ABE9_fragment_3_Cas9n-Nterm, and ABE9-SpRY_fragment_4_SpRY-Cas9n.

470 For the transfection of hiPSCs, pCMV_ABE8e-SpRY and pCMV_ABE9-SpRY were recloned to be
471 expressed under the control of the EF1α promoter. In brief, two fragments were amplified, first the
472 pEF1α_backbone (from pEF1α-hMLH1dn, a gift from David Liu, Addgene Plasmid #174824, (78))
473 and then either ABE8e-SpRY or ABE9-SpRY, for subsequent Gibson assembly cloning.

474 The entire sequence of all constructs assembled using PCR was verified with the PlasmidEZ
475 (Azenta/GeneWiz) full-plasmid sequencing service. All plasmids used for the transfection experiments
476 were prepared using the EndoFree Plasmid Maxi Kit (Qiagen).

477 **Generation of adenine base editor mRNA**

478 mRNA for the microinjection of mouse zygotes for ABE8e-SpRY and ABE9-SpRY was generated by
479 *in vitro* transcription from *SalI*-HF linearised pCMV_ABE8e-SpRY and pCMV_ABE9-SpRY plasmid
480 templates, respectively, using the HiScribe T7 ARCA mRNA Kit. The mRNA was purified using the
481 RNeasy Mini Kit. mRNA quality was confirmed using the TapeStation RNA ScreenTape.

482 **Mammalian cell culture and transfection**

483 Human HEK 293T cells and Neuro2a cells were purchased from ATCC and maintained in Dulbecco's
484 modified Eagle's medium (DMEM; Gibco) supplemented with 10% FBS (Gibco) at 37 °C with 5 %
485 CO_2, up to 20 passages, by passaging cells every two to three days. hiPSCs were purchased from
486 Greenstone Biosciences and cultured on hESC-Qualified Matrix Matrigel-coated (Corning) 6-well
487 plates (Sarstedt) in StemMACS PSC-Brew XF medium (Miltenyi Biotec). Medium was changed daily,
488 and cells were passaged every three days using StemMACS Passaging Solution XF (Miltenyi Biotec).
489 The culture medium was supplemented with 2.5 µM Rock Inhibitor (Y27632, Miltenyi Biotec) on
490 passaging days for 24 hours. The supernatant media from cell cultures were routinely analysed for
491 mycoplasma presence using the MycoSPY Master Mix (Biontex).

492 All HEK293T and N2a transfection experiments were conducted with at least three independent
493 biological replicates. HEK293T and N2a cells were seeded at a density of roughly 110,000 and 180,000
494 cells per well in 24-well plates, respectively, 20-24 hours before transfections. Transfections were
495 performed with 750 ng of base editor plasmid, 250 ng of sgRNA expression plasmid, and, for
496 experiments involving GFP co-transfection, 200 ng of pMAX-GFP (Lonza), combined with 2 µl of
497 Lipofectamine 2000 (Thermo Fisher Scientific) in a total volume of 50 µl Opti-MEM (Thermo Fisher

498 Scientific), according to the manufacturer's instructions. Medium was exchanged to culture medium
499 approximately 24 hours after transfection. For the Orthogonal R-loop assay, HEK293T cells were
500 seeded at a density of 110,000 cells per well in 24-well plates, as described above. However, the cells
501 were co-transfected with a mixture containing 500 ng of plasmids encoding base editor plasmids, 350 ng
502 of *Sp*Cas9 sgRNA (*HEKsite2*), 500 ng of d*Sa*Cas9, 350 ng of *sa*Cas9 sgRNAs targetting separate
503 genomic loci unrelated to the on-target site, and 200 ng of pMAX-GFP (Lonza).

504 hiPSCs were seeded on 6-well plates and transfected after approximately 24 hours at around 60 %
505 confluency. Before transfections, the medium was changed to StemMACS PSC-Brew XF supplemented
506 with StemMACS PSC-Support XF (Miltenyi Biotec). Transfections were performed with 300 ng
507 pEF1α-XMAS-1xStop (a gift from Xiao Wang, Addgene plasmid #164411, (57)), 300 ng pU6-SpCas9-
508 XMAS-1x plasmid, 2100 ng of pEF1α_ABE8e-SpRY or pEF1α_ABE9-SpRY, and 10 µl
509 Lipofectamine Stem (Thermo Fisher Scientific) per well, according to the manufacturer's instructions.
510 Medium was exchanged to culture medium approximately 24 hours after transfection.

511 **Fluorescence-activated cell sorting**

512 Approximately 48 hours after transfections, HEK293T, N2a or hiPSCs were harvested for sorting.
513 HEK293T and N2a cells were treated with TrypLE Express Enzyme (Thermo Fisher Scientific) to
514 singularise the cells, followed by a washing step with D-PBS. The cells were resuspended in buffer
515 containing 1x PBS without Mg^{2+}/Ca^{2+} (Thermo Fisher Scientific), 0.5% FCS (Thermo Fisher Scientific)
516 and 1% Penicillin-Streptomycin and filtered through a 35 µm cell strainer (Corning). hiPSCs were
517 dissociated with Accutase (Thermo Fisher Scientific) and washed with D-PBS, followed by
518 resuspending the cells in 1x PBS without Mg^{2+}/Ca^{2+}, 0.5% FCS, 2.5 µM Rock Inhibitor and passed
519 through a 35 µm cell strainer (Corning). HEK293T and N2a cells co-transfected with pMAX-GFP were
520 sorted for the top 30% GFP-positive population. For the XMAS-TREE reporter assay in hiPSCs, only
521 cells co-expressing GFP and mCherry were sorted. FACS sorting was performed with either a
522 BD FACSAriaIII or BD FACSAria Fusion at the Flow Cytometry & FACS Core Facility (FFCF),
523 Zentrum für Molekulare Biologie der Universität Heidelberg (ZMBH) or FACS Core Facility (dFCCU),
524 Uniklinikum Heidelberg, respectively.

525 **Genomic DNA extraction from mammalian cell culture**

526 After FACS HEK293T, N2a cells were collected in 500 µl DMEM GlutaMAX supplemented with 10%
527 FBS. hiPSCs were collected in 500 µl StemMACS PSC-Brew XF medium supplemented with 2.5 µM
528 Rock Inhibitor. Cells were collected by centrifugation at 20,000 *x* g for 2 minutes, washed with 500 µl
529 D-PBS, and lysed in mammalian gDNA lysis buffer (10 mM Tris-HCl, 0.05% SDS, pH 8, 800 units
530 proteinase K (NEB)) for 2 hours at 37°C to extract genomic DNA. Afterwards, proteinase K was

531 inactivated for 30 min at 80°C. Cells transfected without fluorophore plasmid were washed once 72
532 hours after transfection, and then lysed in mammalian gDNA lysis buffer, as described above.

533 **Microinjection of mouse zygotes**

534 Injections were performed as previously described (79), with minor modifications. In brief, the injection
535 mix contained adenine base editor mRNA (100 ng/µl) and sgRNAs (50 ng/µl each; 12.5 ng/µl each, for
536 pooled sgRNA injections) in injection buffer (10 mM Tris-HCl, 0.25 mM EDTA, pH 7.4) to a final
537 volume of 50 µl with molecular biology-grade water. To prevent clogging of the cannula, the injection
538 mix was filtered shortly before microinjection using a Corning Costar Spin-X 0.22 µm centrifuge tube
539 filter. Zygotes were collected from timed matings and cultured *in vitro* in M2 medium during the
540 injection. Injection into the cytoplasm of zygote-stage embryos was conducted by carefully inserting
541 the injection needle at the equatorial level into the cytoplasm of each embryo, delivering a volume of
542 1-2 picolitres. Subsequently, the embryos were placed in preincubated M16 medium to select lysed and
543 intact embryos. Embryos were transferred on the same day via oviduct transfer to 0.5-day
544 pseudopregnant foster mothers.

545 **Genomic DNA extraction from mouse samples**

546 Embryonic day 14 mice were isolated from surrogate mothers. For DNA extraction, each embryo was
547 sectioned into smaller pieces, and genomic DNA was isolated using the DNeasy Blood & Tissue Kit
548 (Qiagen) following the manufacturer's protocol, with minor modifications. All reagents were applied
549 at double the recommended volume since the starting material exceeded 10 mg per embryo. Proteinase
550 K from New England Biolabs (NEB) was utilised instead of the kit-supplied enzyme.

551 For genotyping of founder mice, ear biopsies were obtained from the Interfakultäre Biomedizinische
552 Forschungseinrichtung of Heidelberg University. Genomic DNA was extracted from ear biopsy
553 samples using a lysis buffer consisting of DirectPCR Lysis Reagent (Mouse Tail) (Viagen Biotech) and
554 0.25 µg/µl Proteinase K (AppliChem). For lysis, each sample was incubated in 100-150 µl of this lysis
555 buffer at 55°C with vigorous shaking for a minimum of 4-5 hours, followed by inactivation of
556 Proteinase K at 85°C for 45 minutes. The lysate is subsequently used directly for PCR.

557 **Off-target analysis in mouse embryos**

558 The top five predicted off-target sites for each target locus were identified using ACEofBASEs (53) as
559 described under sgRNA design (**Supplementary Table 7-10**). ACEofBASEs provides links to
560 Ensembl gene IDs; therefore, the locus information for these sites was extracted from Ensembl.
561 Importantly, the column "distance" in the off-target list was used when exporting Ensembl sequence
562 information. In brief, when navigating the ENSEMBL genome browser, to export the locus information,

563 ensure the value of distance and an additional 1kb is added to the "5' Flanking sequence" and "3'
564 Flanking sequence". Primers were designed (Primer3 2.3.7) to flank the predicted off-target loci.

565 **Targeted deep sequencing and data analysis**

566 Samples were prepared for Amplicon-EZ-based NGS analysis (GeneWiz/Azenta Life Sciences) as
567 previously described (53). All locus-specific primers contained the 5' partial Illumina adapter sequences
568 (Fwd: 5'-ACACTCTTTCCCTACACGACGCTCTTCCGATCT-3', Rev: 5'-
569 GACTGGAGTTCAGACGTGTGCTCTTCCGATCT-3'), and are listed in **Supplementary Table 5**.
570 Typically, samples corresponding to different target loci from each biological replicate were pooled
571 into a single sample. The pooled NGS data were demultiplexed by mapping to the respective reference
572 sequences later.

573 For a higher level of sample multiplexing, a sequencing library with indexing primers that include
574 unique i5 and i7 indexes, as well as P5 and P7 adapter sequences, was established. In brief, following
575 the preparation of PCR amplicons with locus-specific primers as described above (PCR1), a second
576 round of PCR was performed on these amplicons to barcode each sample, thereby allowing for the
577 pooling of samples from both the same and different target sites (PCR2). The primer pairs for the second
578 PCR contain complementary regions to the partial Illumina adapters along with the unique i5 and i7
579 index combinations (**Supplementary Table 6)**. For multiplexing, PCR1 samples were amplified using
580 Q5 Hot Start DNA polymerase (NEB) for 27 cycles, validated by agarose gel electrophoresis of a
581 subsample, and diluted between 1:5 and 1:20 based on gel band density. PCR2 was then set up at a
582 volume of 20 µl, containing 1 µl of the diluted PCR1 product, 0.5 µM of each forward (i5) and reverse
583 primer (i7) to create a combinatorial dual-index library, and Phusion U Green Multiplex PCR Master
584 Mix (Thermo Fisher Scientific); it was amplified for an additional 13 cycles. Individual PCR2
585 amplification was validated by agarose gel electrophoresis of a subsample, and 24 PCR2 samples were
586 pooled, run on a 1% agarose gel, with specific bands excised and cleaned up using the Monarch DNA
587 Gel Extraction Kit (NEB), measured by Qubit 4 Fluorometer (Thermo) using the Qubit dsDNA BR
588 Assay Kit, and pooled to equimolarity totalling 1 µg DNA. Samples were sequenced by GeneWiz
589 (Azenta Life Sciences) using the Sequencing only service with a 5% PhiX spike-in on an Illumina
590 MiSeq with 2 x 250 bp, paired-end sequencing, at a depth of approximately 10 million reads.

591 NGS data (in fastq.gz format) were processed and analysed using CRISPResso2 version 2.2.11 (80). In
592 brief, two types of analyses were run in batch mode. First, all samples were analysed in base editing
593 mode with the following custom input parameters: --min_average_read_quality, 30; --
594 quantification_window_size, 20; --quantification_window_center, -10;
595 --base_editor_output. Downstream analysis was conducted using R version 4.2.1 in R Studio (packages:
596 tidyverse, ggplot, ggpubr, cowplot), with data used to plot Adenines across the protospacer sourced
597 from the "Nucleotide_percentage_summary_around_sgRNA.txt" output file. "Precision"

598 (Supplementary Figure 1) was calculated as previously described (21) by dividing the second highest
599 adenine-based editing frequency by the highest (A5 or A6); for this purpose, the indel frequency was
600 extracted from the "CRISPRessoBatch_quantification_of_editing_frequency.txt" file and calculated as
601 previously described (53).

602 Second, to quantify precise gene editing outcomes, the HDR mode was employed with the following
603 custom input parameters: --min_average_read_quality, 30;
604 --expected_hdr_amplicon_seq; --quantification_window_coordinates, "spacer-7nt (upstream)" –
605 "spacer+PAM sequence (+3nt)"; --discard_indel_reads, TRUE. Downstream analysis was conducted
606 using R, as described above, with data sourced from the
607 "CRISPRessoBatch_quantification_of_editing_frequency.txt" file, with slight modifications following
608 (81). In short, for each sample's HDR amplicon, values under "Reads_aligned_all_amplicons",
609 "Reads_aligned", "Unmodified", "Modified", and "Discarded" (HDR) were collected;
610 additionally, the values under "Discarded" (REF) from the Reference amplicon were obtained. Specific
611 values were then calculated as follows:

612 $$\text{Specified mutation, incl. bystander edits (\%)} = \frac{\text{“Reads_aligned”}}{\text{“Reads_aligned_all_amplicons”}} \times 100 \quad (1)$$

613 $$\text{Specified mutation without bystander edits (\%)} = \frac{\text{“Unmodified”}}{\text{“Reads_aligned_all_amplicons”}} \times 100 \quad (2)$$

614 $$\text{Purity (\%)} = \frac{\text{“Unmodified”}}{\text{“Reads_aligned”}} \times 100 \quad (3)$$

615 $$\text{Indels (\%)} = \frac{\text{“Discarded” (HDR)+ “Discarded” (REF)}}{\text{“Reads_aligned_all_amplicons”}} \times 100 \quad (4)$$

616 **Statistics and graphics**

617 All data reported in the text are presented as mean ± standard deviation (SD). Where appropriate (n≥20),
618 we also reported the median (Q2) and interquartile range (IQR) between the first quartile (Q1) and the
619 third quartile (Q3). Statistical comparisons were conducted using two-tailed Welch's *t*-test, as specified
620 in the figure legends. Details on data reporting, including sample sizes and the statistical methods
621 employed in each experiment, are provided in the figure legends. Data demonstrating statistical
622 significance are depicted in the figures. Analysis and graphical data visualisation were performed in R
623 version 4.2.1 with the Tidyverse, ggplot2, ggpubr, and cowplot packages (82-85). Figures were
624 assembled in Adobe Illustrator, with some icons and schemes imported from Biorender.

ACKNOWLEDGEMENTS

Sayari Bhunia is a member of HBIGS, the Heidelberg Biosciences International Graduate School. We thank the entire Freichel lab for their constructive feedback on the manuscript. We thank Maren Schneider for help with cloning pEF1α_ABE9-SpRY and XMAS-TREE sgRNAs. We thank the whole team from the Interfakultäre Biomedizinische Forschungseinrichtung (IBF) at Heidelberg University for their expert technical assistance. We thank Angela Wirth for writing the animal proposal. While preparing this work, the authors used AI-assisted technologies (Grammarly and ChatGPT) to improve readability and language.

AUTHOR CONTRIBUTIONS

Jun Kai Ong: Conceptualisation, Data curation, Formal analysis, Investigation, Methodology, Validation, Visualisation, Writing – original draft, Writing – review & editing. Sayari Bhunia: Investigation, Validation, Writing – review & editing. Beate Hilbert: Investigation. Vanessa Kirschner: Investigation, Writing – review & editing. Sascha Duglosz: Investigation. Frank Zimmermann: Investigation. Marc Freichel: Conceptualisation, Funding acquisition, Resources, Writing – review & editing. Alex Cornean: Conceptualisation, Data curation, Formal analysis, Methodology, Project administration, Supervision, Visualisation, Writing – original draft, Writing – review & editing.

SUPPLEMENTARY DATA

Supplementary Data will be made available online.

CONFLICT OF INTEREST

Alex Cornean is a co-founder and shareholder of DataHarmony Ltd, a company that provides gene editing-related services and software solutions.

FUNDING

This research was funded by the German Research foundation (DFG) through the Collaborative Research Centres CRC1550 (FKZ 464424253, projects B09 and S01), CRC1328 (335447717, project A21), DFG project FR 1638/5-1 (531047917), the DZHK (German Centre for Cardiovascular Research) and the BMBF (German Ministry of Education and Research); and The Health + Life Science Alliance Heidelberg Mannheim.

DATA AVAILABILITY

Oligonucleotide and sgRNA sequences used in this study are listed in Supplementary Tables 2, 3, 5, and 6. All raw NGS sequencing data generated in this study were in the NCBI Sequence Read Archive (SRA) database as a BioProject with the accession number PRJNA1291991, which will be publicly

656 released upon acceptance, and is available during the review process under the following link:
657 https://dataview.ncbi.nlm.nih.gov/object/PRJNA1291991?reviewer=plb16c7id34365ihronfdvltul

658 pCMV_ABE9-SpRY and pEF1α_ABE9-SpRY will be made available through Addgene. Any other
659 data and reagents will be made available upon reasonable request.

660 **AUTHOR ORCIDS**

661 Jun Kai Ong: https://orcid.org/0009-0005-1865-9465

662 Marc Freichel: https://orcid.org/0000-0003-1387-2636

663 Alex Cornean: http://orcid.org/0000-0003-3727-7057

REFERENCES

1. Williams, R.W. (2006) In Runge, M. S. and Patterson, C. (eds.), *Princ Mol Med*. Humana Press, Totowa, NJ, pp. 53-60. https://doi.org/10.1007/978-1-59259-963-9_8

2. Perlman, R.L. (2016) Mouse models of human disease: An evolutionary perspective. *Evol med public health*, **2016**, 170-176. https://doi.org/10.1093/emph/eow014

3. Smith, P., DiLillo, D.J., Bournazos, S., Li, F. and Ravetch, J.V. (2012) Mouse model recapitulating human Fcγ receptor structural and functional diversity. *Proc Natl Acad Sci USA*, **109**, 6181-6186. https://doi.org/10.1073/pnas.1203954109

4. Scherrer, G., Tryoen-Tóth, P., Filliol, D., Matifas, A., Laustriat, D., Cao, Y.Q., Basbaum, A.I., Dierich, A., Vonesh, J.-L., Gavériaux-Ruff, C. *et al.* (2006) Knockin mice expressing fluorescent δ-opioid receptors uncover G protein-coupled receptor dynamics *in vivo*. *Proc Natl Acad Sci USA*, **103**, 9691-9696. https://doi.org/10.1073/pnas.0603359103

5. Lee, H. (2014) Genetically Engineered Mouse Models for Drug Development and Preclinical Trials. *Biomol Ther*, **22**, 267-274. https://doi.org/10.4062/biomolther.2014.074

6. Passier, R., Orlova, V. and Mummery, C. (2016) Complex Tissue and Disease Modeling using hiPSCs. *Cell Stem Cell*, **18**, 309-321. https://doi.org/10.1016/j.stem.2016.02.011

7. Cong, L., Ran, F.A., Cox, D., Lin, S., Barretto, R., Habib, N., Hsu, P.D., Wu, X., Jiang, W., Marraffini, L.A. *et al.* (2013) Multiplex genome engineering using CRISPR/Cas systems. *Science*, **339**, 819-823. https://doi.org/10.1126/science.1231143

8. Takata, M., Sasaki, M.S., Sonoda, E., Morrison, C., Hashimoto, M., Utsumi, H., Yamaguchi - Iwai, Y., Shinohara, A. and Takeda, S. (1998) Homologous recombination and non - homologous end - joining pathways of DNA double - strand break repair have overlapping roles in the maintenance of chromosomal integrity in vertebrate cells. *EMBO J*, **17**, 5497-5508. https://doi.org/10.1093/emboj/17.18.5497

9. Kosicki, M., Tomberg, K. and Bradley, A. (2018) Repair of double-strand breaks induced by CRISPR–Cas9 leads to large deletions and complex rearrangements. *Nat Biotechnol*, **36**, 765-771. https://doi.org/10.1038/nbt.4192

10. Hwang, G.-H., Lee, S.-H., Oh, M., Kim, S., Habib, O., Jang, H.-K., Kim, H.S., Kim, Y., Kim, C.H., Kim, S. *et al.* (2025) Large DNA deletions occur during DNA repair at 20-fold lower frequency for base editors and prime editors than for Cas9 nucleases. *Nat Biomed Eng*, **9**, 79-92. https://doi.org/10.1038/s41551-024-01277-5

11. Fiumara, M., Ferrari, S., Omer-Javed, A., Beretta, S., Albano, L., Canarutto, D., Varesi, A., Gaddoni, C., Brombin, C., Cugnata, F. *et al.* (2024) Genotoxic effects of base and prime editing in human hematopoietic stem cells. *Nat Biotechnol*, **42**, 877-891. https://doi.org/10.1038/s41587-023-01915-4

12. Gaudelli, N.M., Komor, A.C., Rees, H.A., Packer, M.S., Badran, A.H., Bryson, D.I. and Liu, D.R. (2017) Programmable base editing of A•T to G•C in genomic DNA without DNA cleavage. *Nature*, **551**, 464-471. https://doi.org/10.1038/nature24644

13. Komor, A.C., Kim, Y.B., Packer, M.S., Zuris, J.A. and Liu, D.R. (2016) Programmable editing of a target base in genomic DNA without double-stranded DNA cleavage. *Nature*, **533**, 420-424. https://doi.org/10.1038/nature17946

14. Rees, H.A. and Liu, D.R. (2018) Base editing: precision chemistry on the genome and transcriptome of living cells. *Nat Rev Genet*, **19**, 770-788. https://doi.org/10.1038/s41576-018-0059-1

15. Gaudelli, N.M., Lam, D.K., Rees, H.A., Solá-Esteves, N.M., Barrera, L.A., Born, D.A., Edwards, A., Gehrke, J.M., Lee, S.-J., Liquori, A.J. *et al.* (2020) Directed evolution of adenine base editors with increased activity and therapeutic application. *Nat Biotechnol*, **38**, 892-900. https://doi.org/10.1038/s41587-020-0491-6

16. Wu, X., Scott, D.A., Kriz, A.J., Chiu, A.C., Hsu, P.D., Dadon, D.B., Cheng, A.W., Trevino, A.E., Konermann, S., Chen, S. *et al.* (2014) Genome-wide binding of the CRISPR endonuclease Cas9 in mammalian cells. *Nat Biotechnol*, **32**, 670-676. https://doi.org/10.1038/nbt.2889

17. Hsu, P.D., Scott, D.A., Weinstein, J.A., Ran, F.A., Konermann, S., Agarwala, V., Li, Y., Fine, E.J., Wu, X., Shalem, O. *et al.* (2013) DNA targeting specificity of RNA-guided Cas9 nucleases. *Nat Biotechnol*, **31**, 827-832. https://doi.org/10.1038/nbt.2647

18. Grünewald, J., Zhou, R., Garcia, S.P., Iyer, S., Lareau, C.A., Aryee, M.J. and Joung, J.K. (2019) Transcriptome-wide off-target RNA editing induced by CRISPR-guided DNA base editors. *Nature*, **569**, 433-437. https://doi.org/10.1038/s41586-019-1161-z

19. Li, S., Liu, L., Sun, W., Zhou, X. and Zhou, H. (2022) A large-scale genome and transcriptome sequencing analysis reveals the mutation landscapes induced by high-activity adenine base editors in plants. *Genome Biol*, **23**, 51. https://doi.org/10.1186/s13059-022-02618-w

20. Richter, M.F., Zhao, K.T., Eton, E., Lapinaite, A., Newby, G.A., Thuronyi, B.W., Wilson, C., Koblan, L.W., Zeng, J., Bauer, D.E. *et al.* (2020) Phage-assisted evolution of an adenine base editor with improved Cas domain compatibility and activity. *Nat Biotechnol*, **38**, 883-891. https://doi.org/10.1038/s41587-020-0453-z

21. Chen, L., Zhang, S., Xue, N., Hong, M., Zhang, X., Zhang, D., Yang, J., Bai, S., Huang, Y., Meng, H. *et al.* (2023) Engineering a precise adenine base editor with minimal bystander editing. *Nat Chem Biol*, **19**, 101-110. https://doi.org/10.1038/s41589-022-01163-8

22. Walton, R.T., Christie, K.A., Whittaker, M.N. and Kleinstiver, B.P. (2020) Unconstrained genome targeting with near-PAMless engineered CRISPR-Cas9 variants. *Science*, **368**, 290-296. https://doi.org/10.1126/science.aba8853

23. Liao, J., Chen, S., Hsiao, S., Jiang, Y., Yang, Y., Zhang, Y., Wang, X., Lai, Y., Bauer, D.E. and Wu, Y. (2023) Therapeutic adenine base editing of human hematopoietic stem cells. *Nat Commun*, **14**, 207. https://doi.org/10.1038/s41467-022-35508-7

24. Patel, S. and Kilpatrick, B.S. (2018) Two-pore channels and disease. *Biochimica et Biophysica Acta (BBA) - Molecular Cell Research*, **1865**, 1678-1686. https://doi.org/10.1016/j.bbamcr.2018.05.004

25. García-Rúa, V., Otero, M.F., Lear, P.V., Rodríguez-Penas, D., Feijóo-Bandín, S., Noguera-Moreno, T., Calaza, M., Álvarez-Barredo, M., Mosquera-Leal, A., Parrington, J. *et al.* (2012) Increased Expression of Fatty-Acid and Calcium Metabolism Genes in Failing Human Heart. *PLoS One*, **7**, e37505. https://doi.org/10.1371/journal.pone.0037505

26. Deutsch, R., Kudrina, V., Freichel, M. and Grimm, C. (2025) Two-pore channel regulators - Who is in control? *Frontiers in Physiology*, **Volume 15 - 2024**. https://doi.org/10.3389/fphys.2024.1534071

27. Medert, R., Pironet, A., Bacmeister, L., Segin, S., Londoño, J.E.C., Vennekens, R. and Freichel, M. (2020) Genetic background influences expression and function of the cation channel TRPM4 in the mouse heart. *Basic Res Cardiol*, **115**, 70. https://doi.org/10.1007/s00395-020-00831-x

28. Stallmeyer, B., Zumhagen, S., Denjoy, I., Duthoit, G., Hébert, J.-L., Ferrer, X., Maugenre, S., Schmitz, W., Kirchhefer, U., Schulze-Bahr, E. *et al.* (2012) Mutational spectrum in the Ca2+-activated cation channel gene TRPM4 in patients with cardiac conductance disturbances. *Hum Mutat*, **33**, 109-117. https://doi.org/10.1002/humu.21599

29. Tu, T., Song, Z., Liu, X., Wang, S., He, X., Xi, H., Wang, J., Yan, T., Chen, H., Zhang, Z. *et al.* (2022) A precise and efficient adenine base editor. *Mol Ther*, **30**, 2933-2941. https://doi.org/10.1016/j.ymthe.2022.07.010

30. Jeong, Y.K., Lee, S., Hwang, G.-H., Hong, S.-A., Park, S.-e., Kim, J.-S., Woo, J.-S. and Bae, S. (2021) Adenine base editor engineering reduces editing of bystander cytosines. *Nat Biotechnol*, **39**, 1426-1433. https://doi.org/10.1038/s41587-021-00943-2

31. Cao, X., Guo, J., Huang, S., Yu, W., Li, G., An, L., Li, X., Tao, W., Liu, Q., Huang, X. *et al.* (2022) Engineering of near-PAMless adenine base editor with enhanced editing activity and reduced off-target. *Mol Ther--Nucleic Acids*, **28**, 732-742. https://doi.org/10.1016/j.omtn.2022.04.032

32. Zhang, Z., Tao, W., Huang, S., Sun, W., Wang, Y., Jiang, W., Huang, X. and Lin, C.-P. (2022) Engineering an adenine base editor in human embryonic stem cells with minimal DNA and RNA off-target activities. *Mol Ther--Nucleic Acids*, **29**, 502-510. https://doi.org/10.1016/j.omtn.2022.07.026

33. Li, G., Cheng, Y., Li, Y., Ma, H., Pu, Z., Li, S., Zhao, Y., Huang, X. and Yao, Y. (2023) A novel base editor SpRY-ABE8e^{F148A} mediates efficient A-to-G base editing with a

reduced off-target effect. *Mol Ther--Nucleic Acids*, **31**, 78-87. https://doi.org/10.1016/j.omtn.2022.12.001

34. Xiong, X., Liu, K., Li, Z., Xia, F.-N., Ruan, X.-M., He, X. and Li, J.-F. (2023) Split complementation of base editors to minimize off-target edits. *Nat Plants*, **9**, 1832-1847. https://doi.org/10.1038/s41477-023-01540-8

35. Zeng, H., Yuan, Q., Peng, F., Ma, D., Lingineni, A., Chee, K., Gilberd, P., Osikpa, E.C., Sun, Z. and Gao, X. (2023) A split and inducible adenine base editor for precise in vivo base editing. *Nat Commun*, **14**, 5573. https://doi.org/10.1038/s41467-023-41331-5

36. Kim, Y.-h., Kim, N., Okafor, I., Choi, S., Min, S., Lee, J., Bae, S.-M., Choi, K., Choi, J., Harihar, V. *et al.* (2023) Sniper2L is a high-fidelity Cas9 variant with high activity. *Nat Chem Biol*, **19**, 972-980. https://doi.org/10.1038/s41589-023-01279-5

37. Wang, Z., Yuan, H., Yang, L., Ma, L., Zhang, Y., Deng, J., Li, X., Xiao, W., Li, Z., Qiu, J. *et al.* (2023) Decreasing predictable DNA off-target effects and narrowing editing windows of adenine base editors by fusing human Rad18 protein variant. *International Journal of Biological Macromolecules*, **253**, 127418. https://doi.org/10.1016/j.ijbiomac.2023.127418

38. Hu, J.H., Miller, S.M., Geurts, M.H., Tang, W., Chen, L., Sun, N., Zeina, C.M., Gao, X., Rees, H.A., Lin, Z. *et al.* (2018) Evolved Cas9 variants with broad PAM compatibility and high DNA specificity. *Nature*, **556**, 57-63. https://doi.org/10.1038/nature26155

39. Kleinstiver, B.P., Prew, M.S., Tsai, S.Q., Topkar, V.V., Nguyen, N.T., Zheng, Z., Gonzales, A.P.W., Li, Z., Peterson, R.T., Yeh, J.-R.J. *et al.* (2015) Engineered CRISPR-Cas9 nucleases with altered PAM specificities. *Nature*, **523**, 481-485. https://doi.org/10.1038/nature14592

40. Huang, T.P., Zhao, K.T., Miller, S.M., Gaudelli, N.M., Oakes, B.L., Fellmann, C., Savage, D.F. and Liu, D.R. (2019) Circularly permuted and PAM-modified Cas9 variants broaden the targeting scope of base editors. *Nat Biotechnol*, **37**, 626-631. https://doi.org/10.1038/s41587-019-0134-y

41. Nishimasu, H., Shi, X., Ishiguro, S., Gao, L., Hirano, S., Okazaki, S., Noda, T., Abudayyeh, O.O., Gootenberg, J.S., Mori, H. *et al.* (2018) Engineered CRISPR-Cas9 nuclease with expanded targeting space. *Science*, **361**, 1259-1262. https://doi.org/10.1126/science.aas9129

42. Ran, F.A., Cong, L., Yan, W.X., Scott, D.A., Gootenberg, J.S., Kriz, A.J., Zetsche, B., Shalem, O., Wu, X., Makarova, K.S. *et al.* (2015) In vivo genome editing using Staphylococcus aureus Cas9. *Nature*, **520**, 186-191. https://doi.org/10.1038/nature14299

43. Miller, S.M., Wang, T., Randolph, P.B., Arbab, M., Shen, M.W., Huang, T.P., Matuszek, Z., Newby, G.A., Rees, H.A. and Liu, D.R. (2020) Continuous evolution of SpCas9 variants compatible with non-G PAMs. *Nat Biotechnol*, **38**, 471-481. https://doi.org/10.1038/s41587-020-0412-8

44. Zhao, L., Koseki, S.R.T., Silverstein, R.A., Amrani, N., Peng, C., Kramme, C., Savic, N., Pacesa, M., Rodríguez, T.C., Stan, T. *et al.* (2023) PAM-flexible genome editing with an engineered chimeric Cas9. *Nat Commun*, **14**, 6175. https://doi.org/10.1038/s41467-023-41829-y

45. Li, J., Xu, R., Qin, R., Liu, X., Kong, F. and Wei, P. (2021) Genome editing mediated by SpCas9 variants with broad non-canonical PAM compatibility in plants. *Molecular Plant*, **14**, 352-360. https://doi.org/10.1016/j.molp.2020.12.017

46. Villiger, L., Rothgangl, T., Witzigmann, D., Oka, R., Lin, P.J.C., Qi, W., Janjuha, S., Berk, C., Ringnalda, F., Beattie, M.B. *et al.* (2021) In vivo cytidine base editing of hepatocytes without detectable off-target mutations in RNA and DNA. *Nat Biomed Eng*, **5**, 179-189. https://doi.org/10.1038/s41551-020-00671-z

47. Liu, Z., Lu, Z., Yang, G., Huang, S., Li, G., Feng, S., Liu, Y., Li, J., Yu, W., Zhang, Y. *et al.* (2018) Efficient generation of mouse models of human diseases via ABE- and BE-mediated base editing. *Nat Commun*, **9**, 2338. https://doi.org/10.1038/s41467-018-04768-7

48. Ryu, S.-M., Koo, T., Kim, K., Lim, K., Baek, G., Kim, S.-T., Kim, H.S., Kim, D.-e., Lee, H., Chung, E. *et al.* (2018) Adenine base editing in mouse embryos and an adult mouse model of Duchenne muscular dystrophy. *Nat Biotechnol*, **36**, 536-539. https://doi.org/10.1038/nbt.4148

49. Yang, L., Zhang, X., Wang, L., Yin, S., Zhu, B., Xie, L., Duan, Q., Hu, H., Zheng, R., Wei, Y. *et al.* (2018) Increasing targeting scope of adenosine base editors in mouse and rat embryos through fusion of TadA deaminase with Cas9 variants. *Protein Cell*, **9**, 814-819. https://doi.org/10.1007/s13238-018-0568-x

50. Fu, J., Li, Q., Liu, X., Tu, T., Lv, X., Yin, X., Lv, J., Song, Z., Qu, J., Zhang, J. *et al.* (2021) Human cell based directed evolution of adenine base editors with improved efficiency. *Nat Commun*, **12**, 5897. https://doi.org/10.1038/s41467-021-26211-0

51. Qian, Y., Wang, D., Niu, W., Zhao, D., Li, J., Liu, Z., Gao, X., Han, Y., Lai, L. and Li, Z. (2023) A new compact adenine base editor generated through deletion of HNH and REC2 domain of SpCas9. *BMC Biol*, **21**, 155. https://doi.org/10.1186/s12915-023-01644-9

52. Zhao, D., Gao, X., Zhou, J., Li, J., Qian, Y., Wang, D., Niu, W., Zhang, T., Hu, M., Xiong, H. *et al.* (2023) Engineered domain-inlaid Nme2Cas9 adenine base editors with increased on-target DNA editing and targeting scope. *BMC Biol*, **21**, 250. https://doi.org/10.1186/s12915-023-01754-4

53. Cornean, A., Gierten, J., Welz, B., Mateo, J.L., Thumberger, T. and Wittbrodt, J. (2022) Precise in vivo functional analysis of DNA variants with base editing using ACEofBASEs target prediction. *eLife*, **11**, e72124. https://doi.org/10.7554/eLife.72124

54. Doman, J.L., Raguram, A., Newby, G.A. and Liu, D.R. (2020) Evaluation and minimization of Cas9-independent off-target DNA editing by cytosine base editors. *Nat Biotechnol*, **38**, 620-628. https://doi.org/10.1038/s41587-020-0414-6

55. Joshi, J., Albers, C., Smole, N., Guo, S. and Smith, S.A. (2024) Human induced pluripotent stem cell-derived cardiomyocytes (iPSC-CMs) for modeling cardiac arrhythmias: strengths, challenges and potential solutions. *Frontiers in Physiology*, **Volume 15 - 2024**. https://doi.org/10.3389/fphys.2024.1475152

56. Cerneckis, J., Cai, H. and Shi, Y. (2024) Induced pluripotent stem cells (iPSCs): molecular mechanisms of induction and applications. *Signal Transduction and Targeted Therapy*, **9**, 112. https://doi.org/10.1038/s41392-024-01809-0

57. Brookhouser, N., Nguyen, T., Tekel, S.J., Standage-Beier, K., Wang, X. and Brafman, D.A. (2020) A Cas9-mediated adenosine transient reporter enables enrichment of ABE-targeted cells. *BMC Biol*, **18**, 193. https://doi.org/10.1186/s12915-020-00929-7

58. Rosello, M., Serafini, M., Mignani, L., Finazzi, D., Giovannangeli, C., Mione, M.C., Concordet, J.-P. and Del Bene, F. (2022) Disease modeling by efficient genome editing using a near PAM-less base editor in vivo. *Nat Commun*, **13**, 3435. https://doi.org/10.1038/s41467-022-31172-z

59. Zuo, E., Sun, Y., Wei, W., Yuan, T., Ying, W., Sun, H., Yuan, L., Steinmetz, L.M., Li, Y. and Yang, H. (2019) Cytosine base editor generates substantial off-target single-nucleotide variants in mouse embryos. *Science*, **364**, 289-292. https://doi.org/10.1126/science.aav9973

60. Lee, S.-H., Wu, J., Im, D., Hwang, G.-h., Jeong, Y.K., Jiang, H., Lee, S.J., Jo, D.H., Goddard, W.A., III, Kim, J.H. *et al.* (2025) Bystander editing by adenine base editors impairs vision restoration in a mouse model of Leber congenital amaurosis. *Molecular Therapy Methods & Clinical Development*, **33**. https://doi.org/10.1016/j.omtm.2025.101461

61. Tuladhar, R., Yeu, Y., Tyler Piazza, J., Tan, Z., Rene Clemenceau, J., Wu, X., Barrett, Q., Herbert, J., Mathews, D.H., Kim, J. *et al.* (2019) CRISPR-Cas9-based mutagenesis frequently provokes on-target mRNA misregulation. *Nat Commun*, **10**, 4056. https://doi.org/10.1038/s41467-019-12028-5

62. Höijer, I., Emmanouilidou, A., Östlund, R., van Schendel, R., Bozorgpana, S., Tijsterman, M., Feuk, L., Gyllensten, U., den Hoed, M. and Ameur, A. (2022) CRISPR-Cas9 induces large structural variants at on-target and off-target sites in vivo that segregate across generations. *Nat Commun*, **13**, 627. https://doi.org/10.1038/s41467-022-28244-5

63. Liao, J., Zhang, H., Chen, S., Hsiao, S., Lai, C., Feng, H., Ren, W., Feng, C., Xie, D., Zheng, Y. *et al.* (2025) Sequential Amino Acid Mutagenesis-Driven De Novo Evolution of Adenine Deaminases Enables Efficient In Vivo Base Editing in Primate. *bioRxiv*, 2025.2005.2014.653640. https://doi.org/10.1101/2025.05.14.653640/

64. Xiao, Y.-L., Wu, Y. and Tang, W. (2024) An adenine base editor variant expands context compatibility. *Nat Biotechnol*, **42**, 1442-1453. https://doi.org/10.1038/s41587-023-01994-3

65. Qin, W., Liang, F., Lin, S.-J., Petree, C., Huang, K., Zhang, Y., Li, L., Varshney, P., Mourrain, P., Liu, Y. *et al.* (2024) ABE-ultramax for high-efficiency biallelic adenine base editing in zebrafish. *Nat Commun*, **15**, 5613. https://doi.org/10.1038/s41467-024-49943-1

66. Perrotta, R.M., Vinke, S., Ferreira, R., Moret, M., Mahas, A., Chiappino-Pepe, A., Riedmayr, L.M., Mehra, A.-T., Lehmann, L.S. and Church, G.M. (2024) Machine Learning and Directed Evolution of Base Editing Enzymes. *bioRxiv*, 2024.2005.2017.594556. https://doi.org/10.1101/2024.05.17.594556

67. Zhao, N., Zhou, J., Tao, T., Wang, Q., Tang, J., Li, D., Gou, S., Guan, Z., Olajide, J.S., Lin, J. *et al.* (2024) Evolved cytidine and adenine base editors with high precision and minimized off-target activity by a continuous directed evolution system in mammalian cells. *Nat Commun*, **15**, 8140. https://doi.org/10.1038/s41467-024-52483-3

68. Chen, Q., Sun, Y., Yao, J., Lu, Y., Qiu, R., Zhou, F., Deng, Z. and Sun, Y. (2025) Engineering of Peptide-Inserted Base Editors with Enhanced Accuracy and Security. *Small*, **21**, 2411583. https://doi.org/10.1002/smll.202411583

69. Silverstein, R.A., Kim, N., Kroell, A.-S., Walton, R.T., Delano, J., Butcher, R.M., Pacesa, M., Smith, B.K., Christie, K.A., Ha, L.L. *et al.* (2025) Custom CRISPR–Cas9 PAM variants via scalable engineering and machine learning. *Nature*. https://doi.org/10.1038/s41586-025-09021-y

70. Peña-Gutiérrez, I., Olalla-Sastre, B., Río, P. and Rodríguez-Madoz, J.R. (2025) Beyond precision: evaluation of off-target clustered regularly interspaced short palindromic repeats/Cas9–mediated genome editing. *Cytotherapy*, **27**, 279-286. https://doi.org/10.1016/j.jcyt.2024.10.010

71. Shi, Y., Inoue, H., Wu, J.C. and Yamanaka, S. (2017) Induced pluripotent stem cell technology: a decade of progress. *Nature Reviews Drug Discovery*, **16**, 115-130. https://doi.org/10.1038/nrd.2016.245

72. Liu, C., Oikonomopoulos, A., Sayed, N. and Wu, J.C. (2018) Modeling human diseases with induced pluripotent stem cells: from 2D to 3D and beyond. *Development*, **145**. https://doi.org/10.1242/dev.156166

73. Heinzelmann, E., Piraino, F., Costa, M., Roch, A., Norkin, M., Garnier, V., Homicsko, K. and Brandenberg, N. (2024) iPSC-derived and Patient-Derived Organoids: Applications and challenges in scalability and reproducibility as pre-clinical models. *Current Research in Toxicology*, **7**, 100197. https://doi.org/10.1016/j.crtox.2024.100197

74. Chang, Y., Lan, F., Zhang, Y. and Ma, S. (2024) Crispr-Based Editing of Human Pluripotent Stem Cells for Disease Modeling. *Stem Cell Reviews and Reports*, **20**, 1151-1161. https://doi.org/10.1007/s12015-024-10713-7

75. Nami, F., Ramezankhani, R., Vandenabeele, M., Vervliet, T., Vogels, K., Urano, F. and Verfaillie, C. (2021) Fast and Efficient Generation of Isogenic Induced Pluripotent Stem Cell Lines Using Adenine Base Editing. *The CRISPR Journal*, **4**, 502-518. https://doi.org/10.1089/crispr.2021.0006

76. Anzalone, A.V., Randolph, P.B., Davis, J.R., Sousa, A.A., Koblan, L.W., Levy, J.M., Chen, P.J., Wilson, C., Newby, G.A., Raguram, A. *et al.* (2019) Search-and-replace genome editing without double-strand breaks or donor DNA. *Nature*, **576**, 149-157. https://doi.org/10.1038/s41586-019-1711-4

77. Alves, C.R.R., Ha, L.L., Yaworski, R., Sutton, E.R., Lazzarotto, C.R., Christie, K.A., Reilly, A., Beauvais, A., Doll, R.M., de la Cruz, D. *et al.* (2024) Optimization of base editors for the functional correction of SMN2 as a treatment for spinal muscular atrophy. *Nat Biomed Eng*, **8**, 118-131. https://doi.org/10.1038/s41551-023-01132-z

78. Chen, P.J., Hussmann, J.A., Yan, J., Knipping, F., Ravisankar, P., Chen, P.-F., Chen, C., Nelson, J.W., Newby, G.A., Sahin, M. *et al.* (2021) Enhanced prime editing systems by manipulating cellular determinants of editing outcomes. *Cell*, **184**, 5635-5652.e5629. https://doi.org/10.1016/j.cell.2021.09.018

79. Medert, R., Thumberger, T., Tavhelidse-Suck, T., Hub, T., Kellner, T., Oguchi, Y., Dlugosz, S., Zimmermann, F., Wittbrodt, J. and Freichel, M. (2022) Efficient single copy integration via homology-directed repair (scHDR) by 5′ modification of large DNA donor fragments in mice. *Nucleic Acids Res*, **51**, e14-e14. https://doi.org/10.1093/nar/gkac1150

80. Clement, K., Rees, H., Canver, M.C., Gehrke, J.M., Farouni, R., Hsu, J.Y., Cole, M.A., Liu, D.R., Joung, J.K., Bauer, D.E. *et al.* (2019) CRISPResso2 provides accurate and rapid genome editing sequence analysis. *Nat Biotechnol*, **37**, 224-226. https://doi.org/10.1038/s41587-019-0032-3

81. Doman, J.L., Sousa, A.A., Randolph, P.B., Chen, P.J. and Liu, D.R. (2022) Designing and executing prime editing experiments in mammalian cells. *Nature Protocols*, **17**, 2431-2468. https://doi.org/10.1038/s41596-022-00724-4

82. Wickham, H., Averick, M., Bryan, J., Chang, W., McGowan, L., François, R., Grolemund, G., Hayes, A., Henry, L., Hester, J. *et al.* (2019) Welcome to the tidyverse. *J Open Source Softw*, **4**, 1686. http://dx.doi.org/10.21105/joss.01686

83. Wickham, H. (2016) ggplot2: Elegant Graphics for Data Analysis. *Springer-Verlag New York*. https://doi.org/10.18637/jss.v035.b01

84. Kassambara, A. (2022) ggpubr: 'ggplot2' Based Publication Ready Plots. https://doi.org/10.32614/CRAN.package.ggpubr

85. Wilke, C.O. (2024) cowplot: Streamlined Plot Theme and Plot Annotations for 'ggplot2'. https://doi.org/10.32614/CRAN.package.cowplot

TABLES AND FIGURES

FIGURES

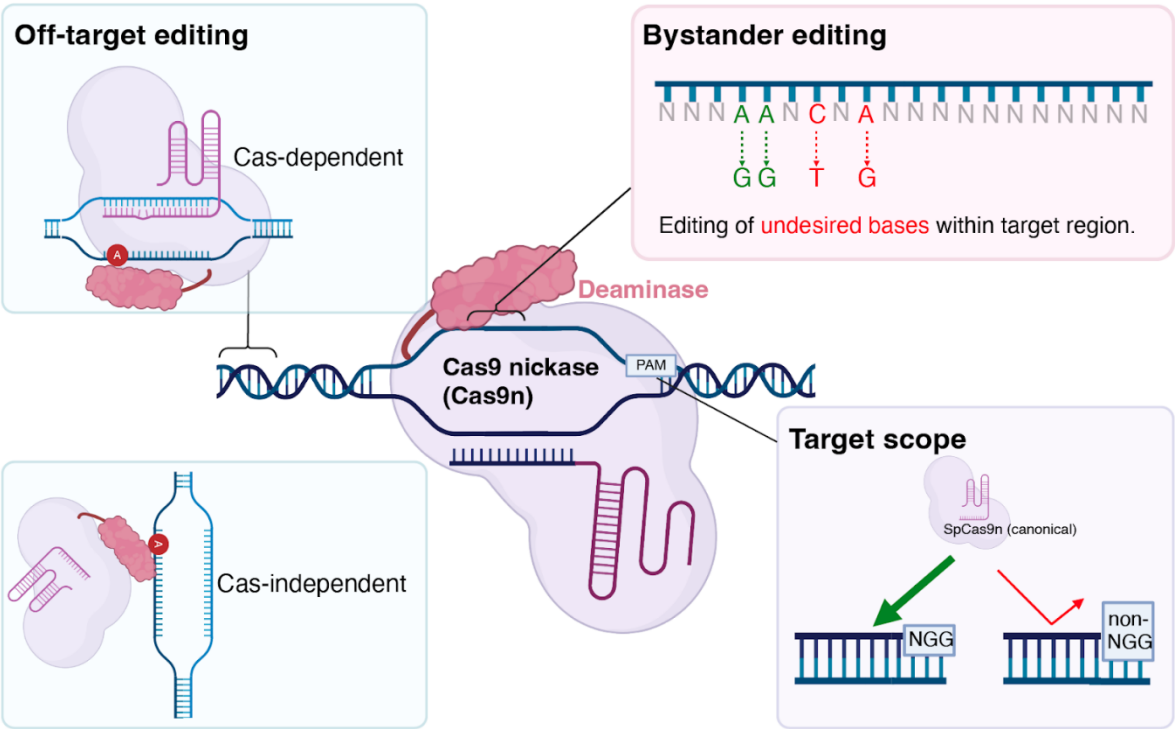

Figure 1. Limitations of disease modelling with ABEs. Schematic of limitations of ABEs in generating disease models. ABEs can have Cas-dependent or -independent off-target editing. Besides targeted adenines, ABEs also have bystander activity on non-target bases. SpCas9 employed in ABEs recognises a 3' NGG PAM while does not bind optimally, or at all, to non-NGG PAM sites. This Figure was partially prepared with BioRender.

Figure 2

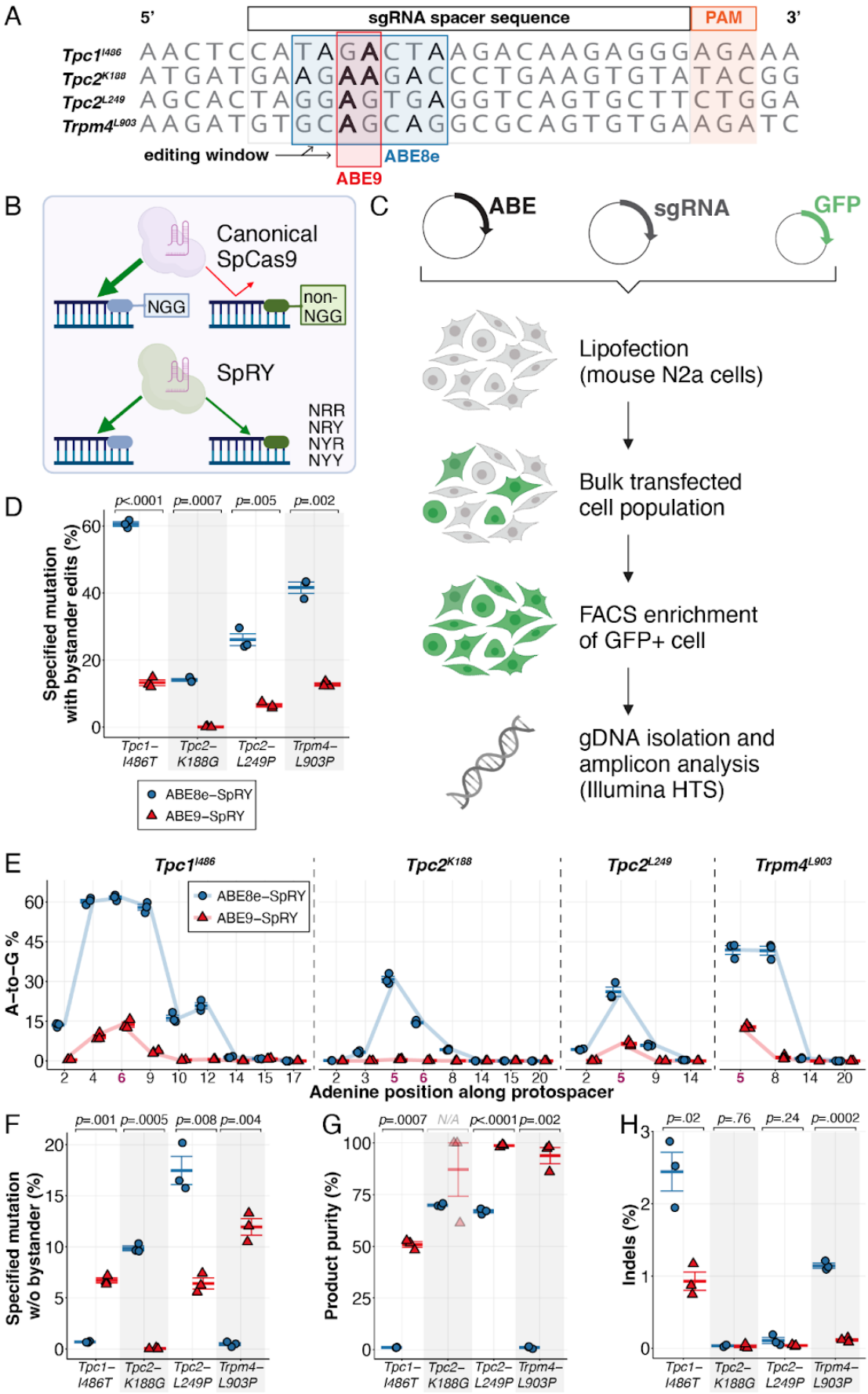
A
5'
sgRNA spacer sequence
PAM
3'
Tpc1I486 AACTCCATAGACTAAGACAAGAGGGAGAAA
Tpc2K188 ATGATGAAGAAGACCCTGAAGTGTATACGG
Tpc2L249 AGCACTAGGAGTGAGGTCAGTGCTTCTGGA
Trpm4L903 AAGATGTGCAGCAGGCGCAGTGTGAAGATC
editing window
ABE8e
ABE9
B
Canonical SpCas9
NGG
non-NGG
SpRY
NRR
NRY
NYR
NYY
C
ABE
sgRNA
GFP
Lipofection (mouse N2a cells)
Bulk transfected cell population
FACS enrichment of GFP+ cell
gDNA isolation and amplicon analysis (Illumina HTS)
D
p<.0001
p=.0007
p=.005
p=.002
Specified mutation with bystander edits (%)
Tpc1–I486T
Tpc2–K188G
Tpc2–L249P
Trpm4–L903P
ABE8e–SpRY
ABE9–SpRY
E
Tpc1I486
Tpc2K188
Tpc2L249
Trpm4L903
A–to–G %
Adenine position along protospacer
F
p=.001
p=.0005
p=.008
p=.004
Specified mutation w/o bystander (%)
G
p=.0007
N/A
p<.0001
p=.002
Product purity (%)
H
p=.02
p=.76
p=.24
p=.0002
Indels (%)

Figure 2. Evaluation of ABE-SpRY constructs in target sites of interest in mouse N2a cells. A, Design of sgRNAs for optimal adenine base editing. Target adenines (bolded in red) for each locus are positioned within the optimal editing windows of ABE8e and ABE9 deaminases with the corresponding PAM sites shown. **B,** The Cas9 variant SpRY can target non-NGG PAM sites, unlike the wild-type SpCas9. **C,** N2a cells were co-transfected with three plasmids: the ABE plasmid, sgRNA plasmid, and GFP plasmid. GFP-positive cells were sorted, and genomic DNA (gDNA) was extracted for subsequent targeted sequencing analysis. **D,** Maximum editing efficiency observed for the target adenine using ABE8e- or ABE9-SpRY, regardless of bystander editing. **E,** A-to-G editing efficiencies of ABE8e and ABE9-SpRY at each adenine position along the protospacer region for the four target sites. The positions of adenines of interest are bolded in red. **F,** Editing efficiency of the target adenine using ABE8e- or ABE9-SpRY, considering only reads without bystander editing or indels. **G,** Product purity, calculated as the proportion of correctly edited sequences (F) relative to the total editing events (D), expressed as a percentage (F/D × 100%). **H,** Frequency of indels at each of the four target sites. Data is presented as mean ± s.e.m., and individual data points are shown for three biological replicates. Parts of the schematics in **C** were created with BioRender.com.

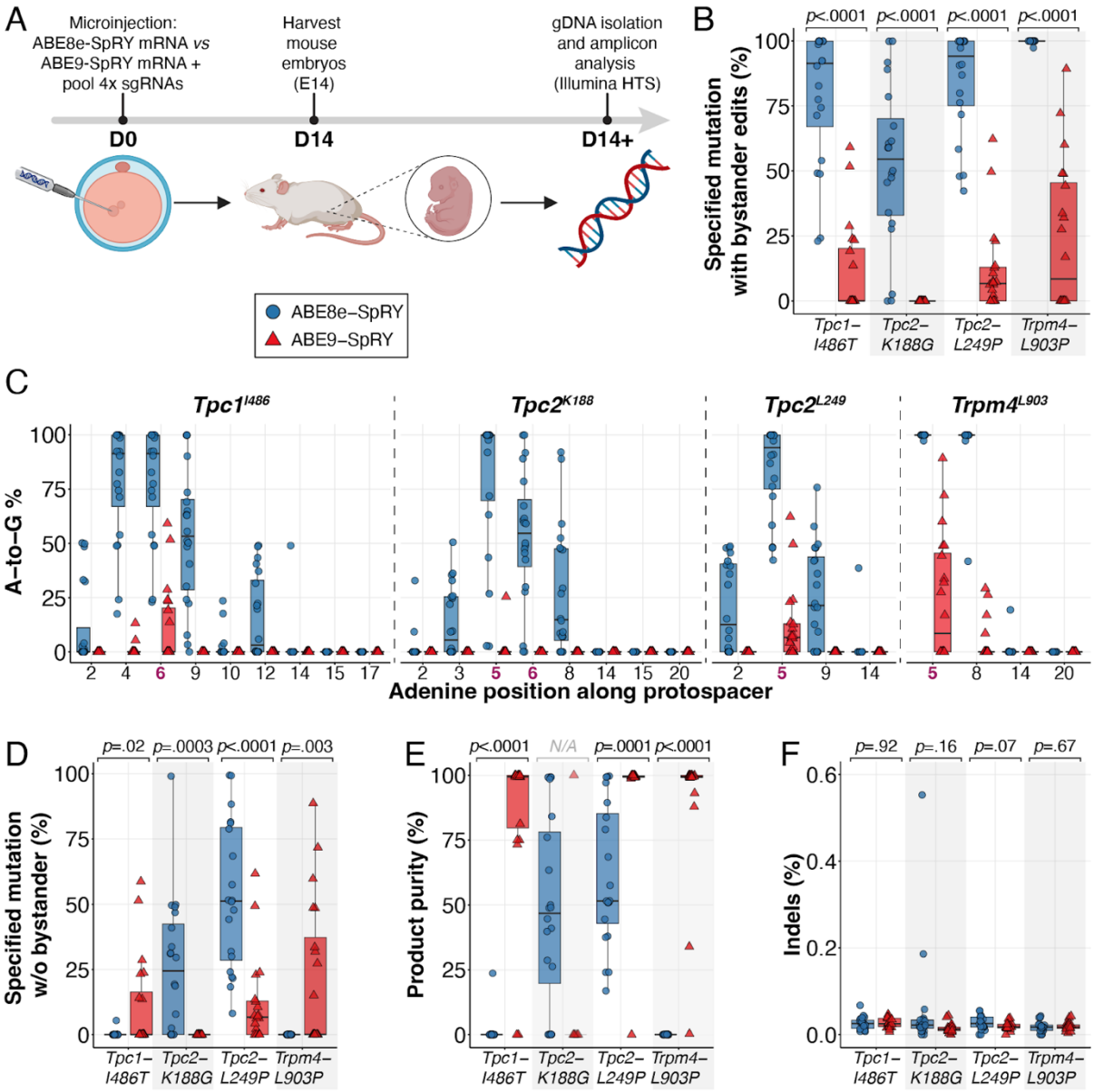

Figure 3. Evaluation of ABE-SpRY constructs in target sites of interest in mouse embryos. A, Schematic of generation of genetically edited mouse embryos. **B,** Maximum editing efficiency observed for the target adenine, regardless of bystander editing. **C,** A-to-G editing frequencies in twenty ABE8e or ABE9-SpRY edited mouse embryos at each adenine position along the protospacer region for the four target sites. Target adenines are bolded in red. **D,** Maximum desired editing efficiency excluding cases with bystander editing. **E,** Product purity, calculated as the proportion of correctly edited sequences (D) relative to the total editing events (B), expressed as a percentage (D/B × 100%). **F,** Frequency of indel occurrence at the four target sites. Data are displayed as standard boxplots following the Tukey convention, including the median (horizontal line), and individual data points are shown for 20 independent biological replicates. Parts of the schematics in **A** were created with BioRender.com.

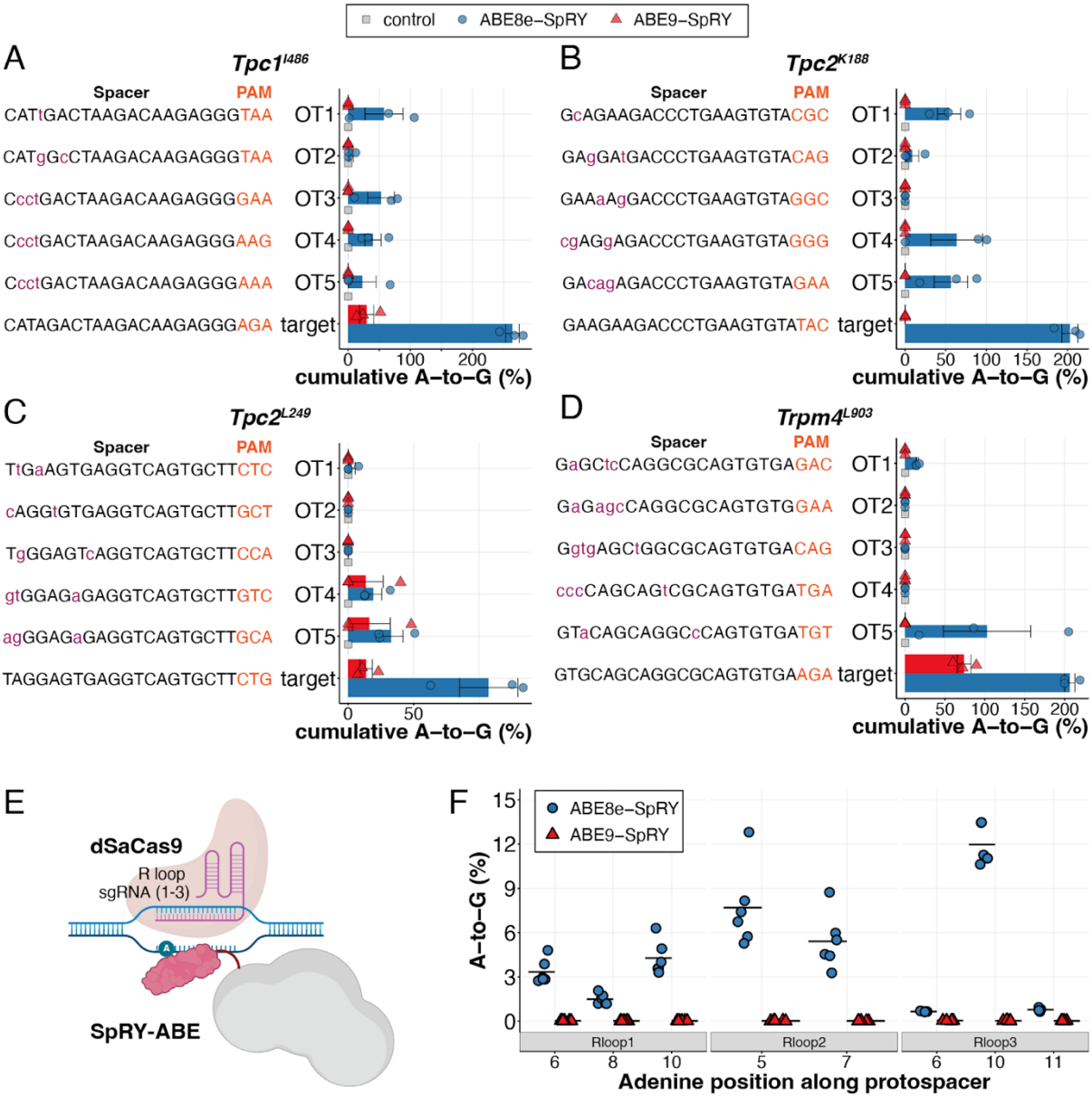

Figure 4. Off-target mutation analysis of ABE-SpRY constructs. A-D, Evaluation of cumulative on- and off-target DNA editing by ABE8e- and ABE9-SpRY in mouse embryos in a Cas9-dependent manner. Data represents mean ± s.e.m. from three biological replicates. **E,** Diagram of the R-loop assay illustrating how the base editor can target transient non-target R-loops formed by dSaCas9. **F,** Cas9-independent assessment of off-target DNA editing by ABE8e-SpRY and ABE9-SpRY, using the orthogonal R-loop assay at specific R-loop sites with five or six biological replicates. The black horizontal bar shows the mean at each adenine position grouped by editor. Parts of the schematics in **E** were created with BioRender.com.

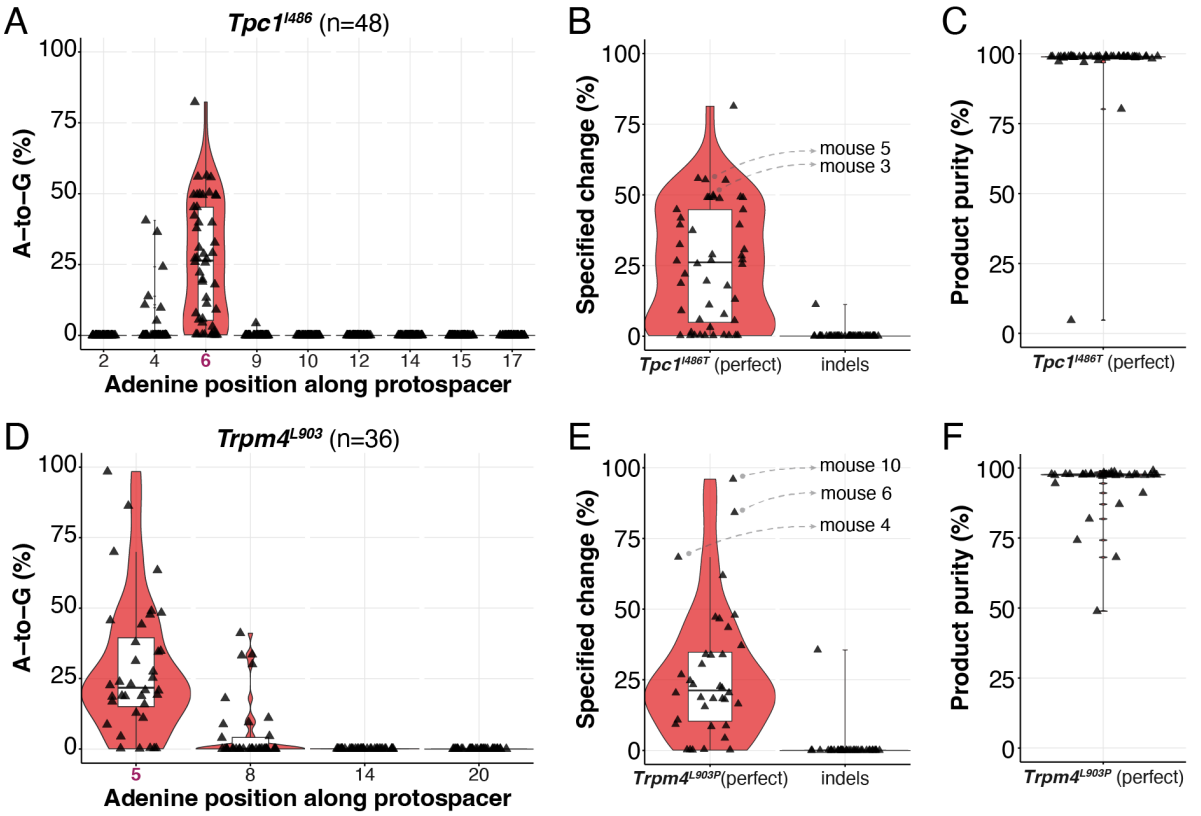

G

Tpc1 p.I486T

F0 ♂		F0 ♀
mouse 3	X	C57BL/6N
mouse 5	X	C57BL/6N

→

F1 id	n	+/+	+/-	%	F1 ♂		F1 ♀
m3-F1	8	3	5	62.5	m3-F1_6 (+/-)	X	C57BL/6N
m5-F1	9	4	5	55.6	m3-F1_7 (+/-)	X	C57BL/6N
					m5-F1_7 (+/-)	X	C57BL/6N

→

F2 id	n	+/+	+/-	%
m3_6-F2	9	6	3	33.3
m3_7-F2	6	3	3	50
m5_7-F2	7	6	1	14.3

H

Trpm4 p.L903P

F0 ♂		F0 ♀
mouse 4	X	C57BL/6N
mouse 6	X	C57BL/6N
mouse 10	X	C57BL/6N

→

F1 id	n	+/+	+/-	%	F1 ♂		F1 ♀
m4-F1	10	2	8	80	m4-F1_6 (+/-)	X	C57BL/6N
m6-F1	9	0	9	100	m6-F1_7 (+/-)	X	C57BL/6N
m10-F1	4	0	4	100			

→

F2 id	n	+/+	+/-	%
m4_6-F2	10	5	5	50
m6_7-F2	7	6	1	14.3

Figure 5. ABE9-SpRY can effectively produce *Tpc1*^{I486T} and *Trpm4*^{L903P} founder mice. A-to-G editing frequencies plotted across each adenine position are shown in **A,** for 48 *Tpc1*^{I486} adult mouse biopsies, and **D,** for 36 *Trpm4*^{L903} adult mouse biopsies. The frequency of desired editing (without bystander edits) and indels are presented in **B,** for *Tpc1*^{I486} adults, and **E,** for *Trpm4*^{L903} adult mice. Product purity is calculated as the percentage of correctly edited sequences relative to the total number of modified alleles and is displayed in **C**, for *Tpc1*^{I486} adults, and **F,** for *Trpm4*^{L903} adult mice. Data are presented as standard boxplots (white) following the Tukey convention, which includes the median (black horizontal line), displayed within violin plots (red), and individual data points (black) representing each biological replicate. Crossing schemes of F0 founder mice, with numerical data for F1 and F2 transmission for *Tpc1*^{I486T} (**G**), and *Trpm4*^{L903P} (**H**), respectively.

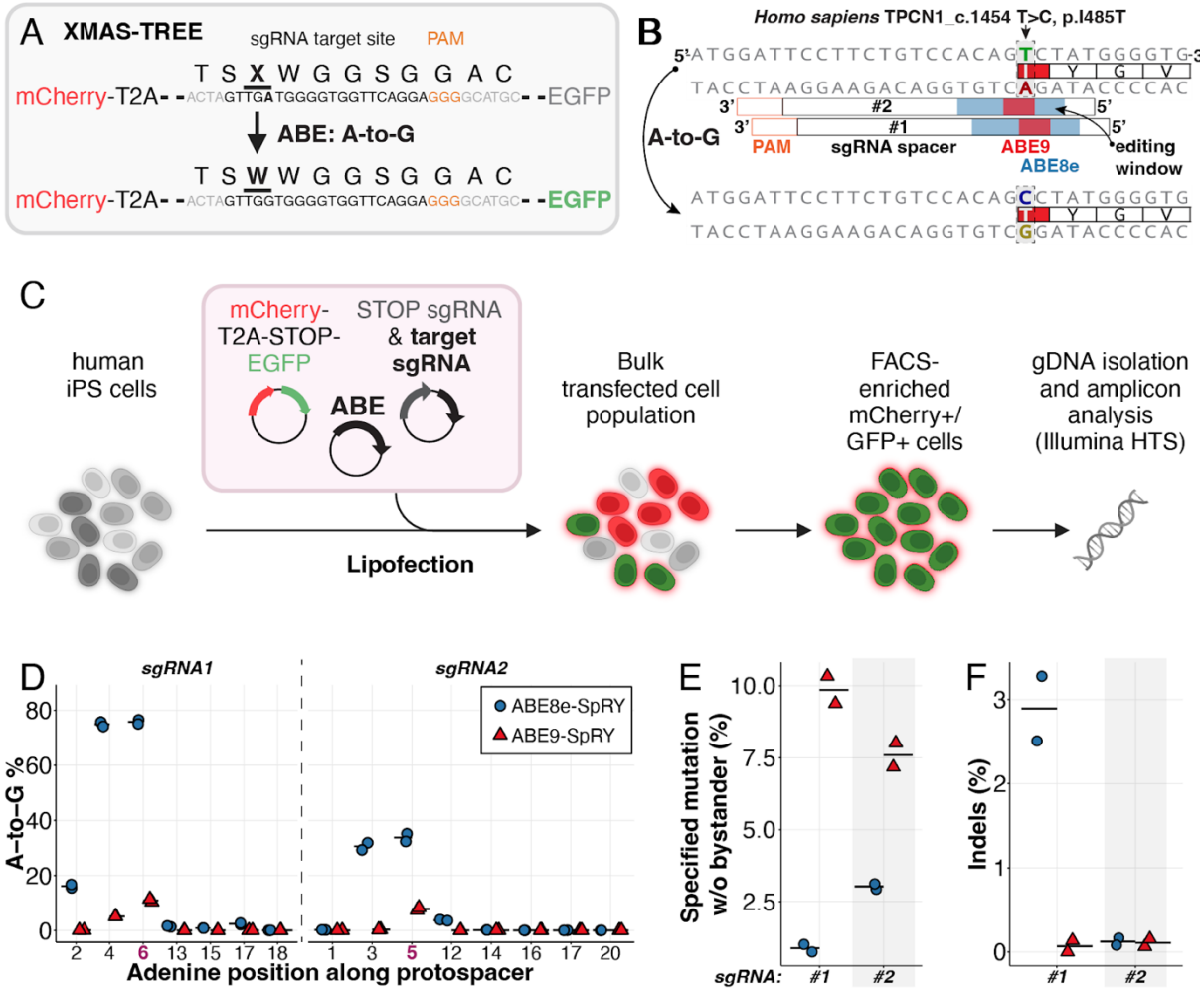

Figure 6. Enrichment and analysis of base-edited hiPSC populations via XMAS-TREE. A, Diagram of the X-MAS TREE system, illustrating the expression of an mCherry cassette followed by a stop codon (TGA) and a GFP cassette. Conversion of the adenine in the stop codon to guanine activates GFP expression. **B,** Diagram showing the tiling of two sgRNAs across the target genomic region. **C,** Schematic of the X-MAS TREE workflow for identifying and enriching adenine base-edited cells. Flow cytometry was used to isolate populations that are double-positive for mCherry and GFP for downstream sequencing. **(D)** Percentage of adenine-to-guanine conversions along the protospacer; **(E)** percentage of desired edits without bystander effects; and **(F)** percentage of indels observed with ABE8e-SpRY or ABE9-SpRY, using sgRNA1 or sgRNA2 in sorted cells. Horizontal bars represent the mean from two biological replicates. Parts of the schematics in **C** were created with BioRender.com.

Tables

Table 1. Overview of available approaches to overcome precision, off-target (OT) and targetability issues.

Goal	Type	Editor	Efficiency *	Editing window (vs 3-10*)	Off-targets*	Ref
Precision	Deaminase mutations	ABE9e-NG (R111T ,N127K, Q154R)	Similar	(3)4-7(8) at similar activity		(29)
		ABE8e-N108Q	Similar	4-7	**reduced DNA and RNA OTs**	
		ABE9 (N108Q, L145T)	**> -20%**	**5-6**		**(21)**
	Split editor	PIGS-ABE8e	> -40%	4-9	reduced DNA and RNA OTs	(34)
		sABE v3.22	> -25%	4-7		(35)
	Effector domain	ABE8e-e18	> -10%	5-7	reduced DNA OTs	(37)
Off-target reduction	Deaminase mutations	ABE8e-V106W	Similar	Similar	Reduction of DNA & RNA OTs	(20)
		ABE8.17-m-V106W	> -10%	Similar		(15)
		ABE8e-WA	Similar	4-8	Reduced RNA OTs	(30)
		ABE8e-WQ	> -20%	4-8		
	Deaminase mutation (+ Cas9 variant)	SpRY-ABE8e-F148A	Similar	Similar	Reduced RNA OTs	(33)
		CE-ABE8e-SpRY	Similar	Similar	Slightly reduced DNA OTs and reduced RNA OTs	(31)
		CE-ABE8e-dV-SpRY	Similar	Similar	Reduced indels, RNA and DNA OTs	(32)
	Cas9 variant	Sniper2L	Low mismatch tolerance (only 1 tolerated)			(36)
Target-ability	Cas9 variant	**ABEmax-SpRY**	**PAMless; targetability across NNN PAMs but likely massive increase in DNA OTs**			**(22)**
		ABE8e-SpRYc	PAMless; at certain selected loci more unbiased than ABE8e-SpRY			(44)

* mostly compared to ABE8e.

SUPPLEMENTARY FIGURES

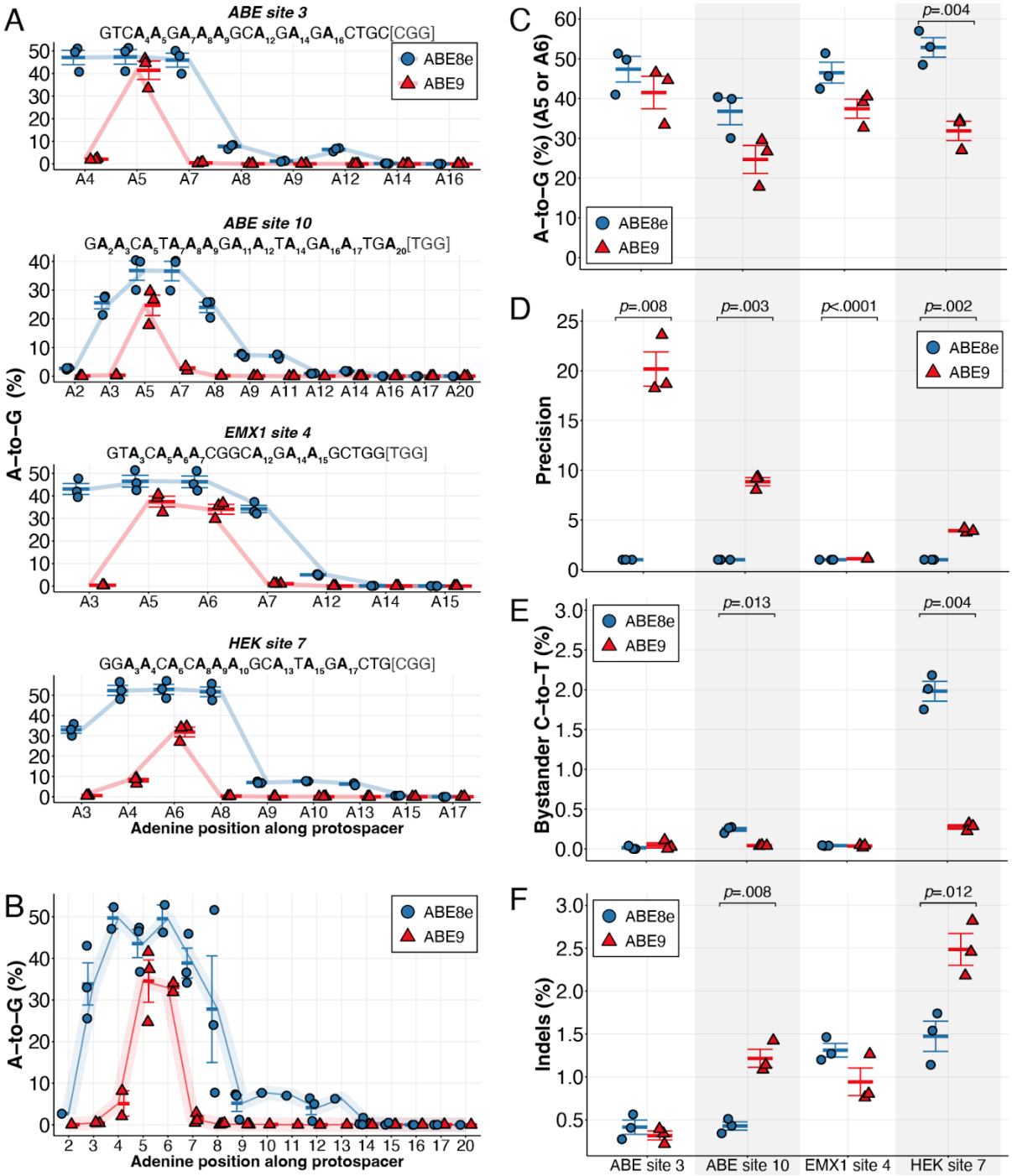

Supplementary Figure 1. ABE9's precision outweighs the higher A-to-G efficiency of ABE8e in human cells. A, Editing efficiencies of ABE8e and ABE9 across four endogenous target sites. **B,** Summary plot of editing window across the four loci. **C,** A-to-G editing frequency at adenine positions A5 or A6 (the highest is considered) at the four target sites. **D,** Precision (according to Chen et al. 2023, *Nat Chem Biol*) calculated by dividing the highest A-to-G editing frequency at A5 (*ABE site 3, ABE site 10, EMX1 site 4)* or A6 (*HEK site 7*) by the second highest frequency at A4, A7, A6, and A4 for *ABE site 3, ABE site 10, EMX1 site 4*, and *HEK site 7*, respectively. **E,** Unwanted C-to-T editing frequency measured across the protospacer sequence. **F,** Indel frequency across the target sites. Error bars represent mean ± s.e.m. and individual data points for three independent biological replicates are shown. Statistical significance was determined by two-tailed Welch's *t*-test.

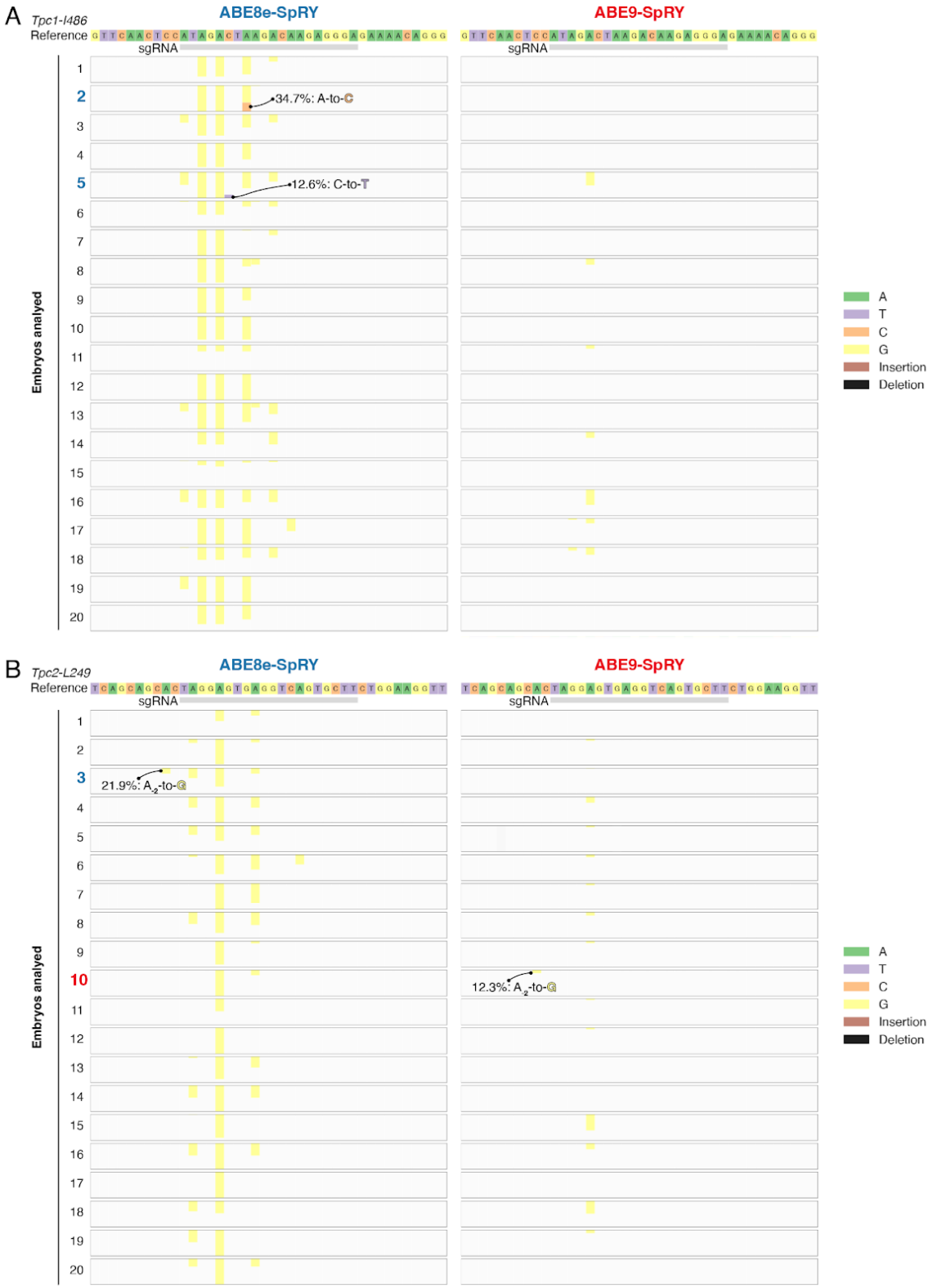

Supplementary Figure 2. Undesired on-target editing with ABE8e-SpRY and ABE9-SpRY at the *Tpc1*^{I486} (A) and *Tpc2*^{L249} (B) loci. Graphs show the base composition in Crispresso2 plots of NGS analysis, highlighting, in colour, any modifications in edited embryos compared to the reference sequence 10 bp downstream and upstream of the sgRNA target site. The vertical size corresponds to the frequency of the modification.

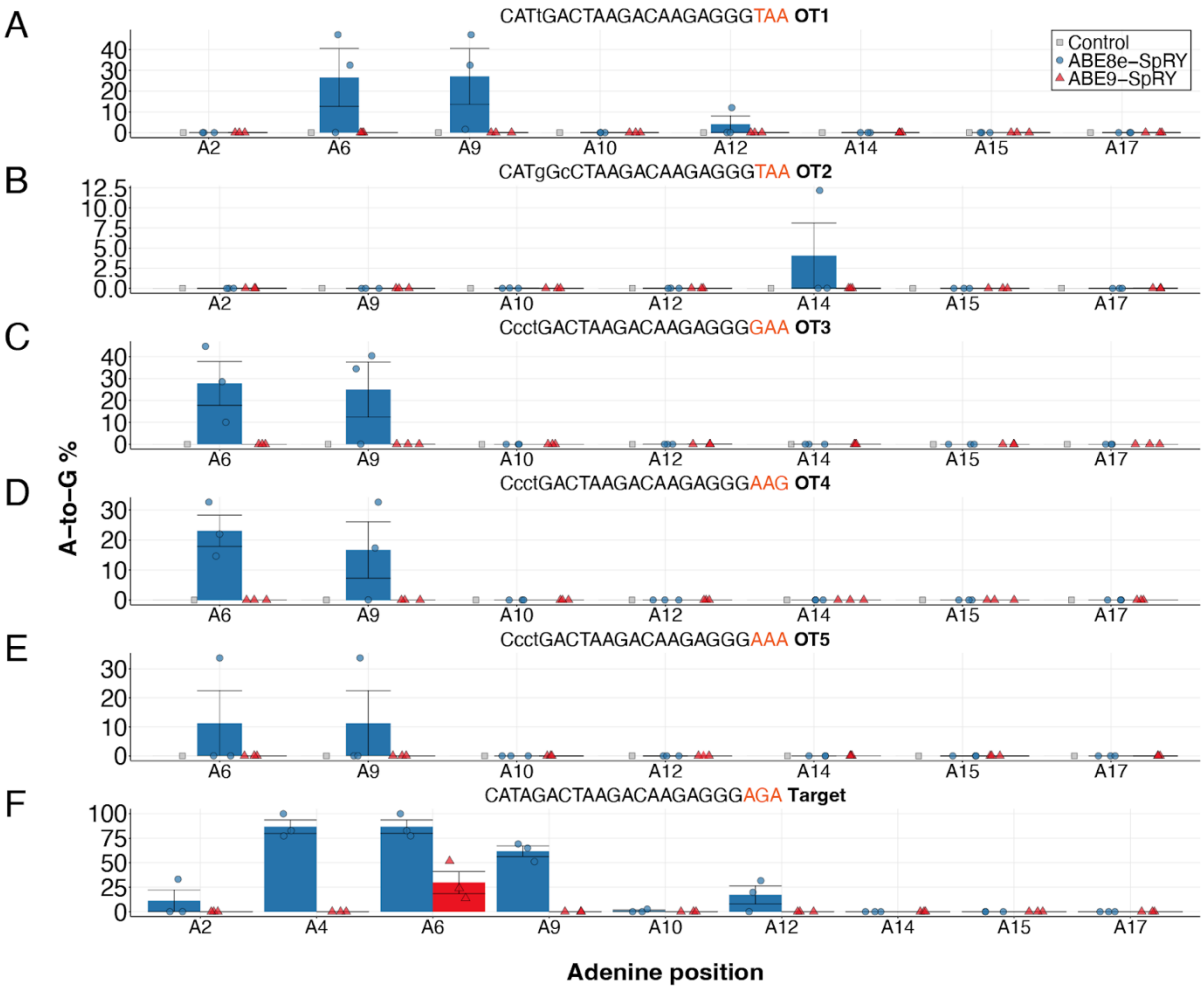

Supplementary Figure 3. ***Tpc1*^{I486} off-target analysis. A-E,** A-to-G frequency analysis of the top five predicted off-target site across all adenines within the protospacer sequence. Mismatches compared to the on-target sequence (**F**) are shown by lowercase letters while the PAM sequence is highlighted in orange. **F,** Replotting of the on-target A-to-G editing efficiency for the embryos used for off-target evaluation (Fig. 3C). Error bars represent mean ± s.e.m. and individual data points for three independent biological replicates are shown.

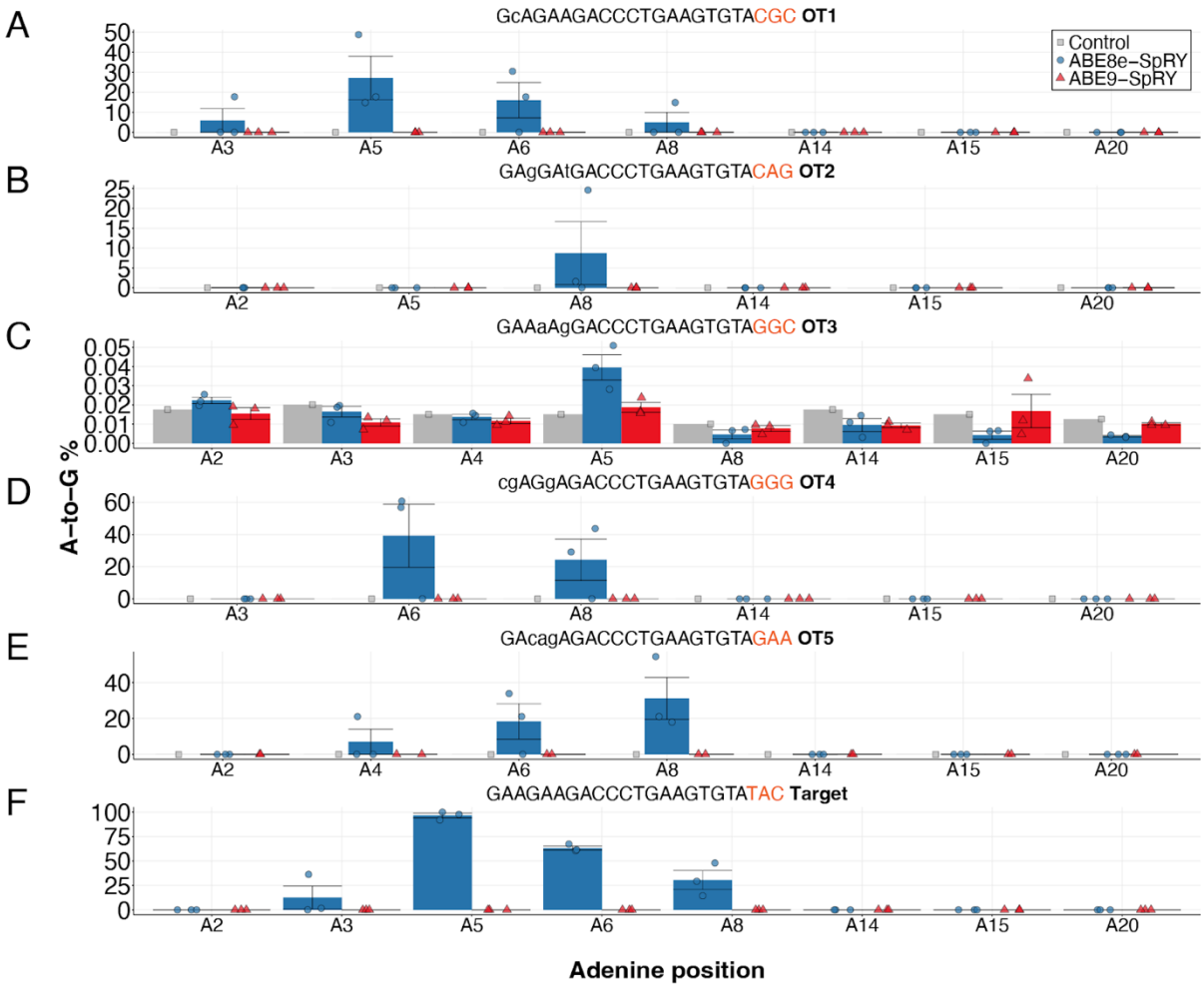

Supplementary Figure 4. ***Tpc2^{K188}*** **off-target analysis. A-E,** A-to-G frequency analysis of the top five predicted off-target site across all adenines within the protospacer sequence. Mismatches compared to the on-target sequence (**F**) are shown by lowercase letters while the PAM sequence is highlighted in orange. **F,** Replotting of the on-target A-to-G editing efficiency for the embryos used for off-target evaluation (Fig. 3C). Error bars represent mean ± s.e.m. and individual data points for three independent biological replicates are shown.

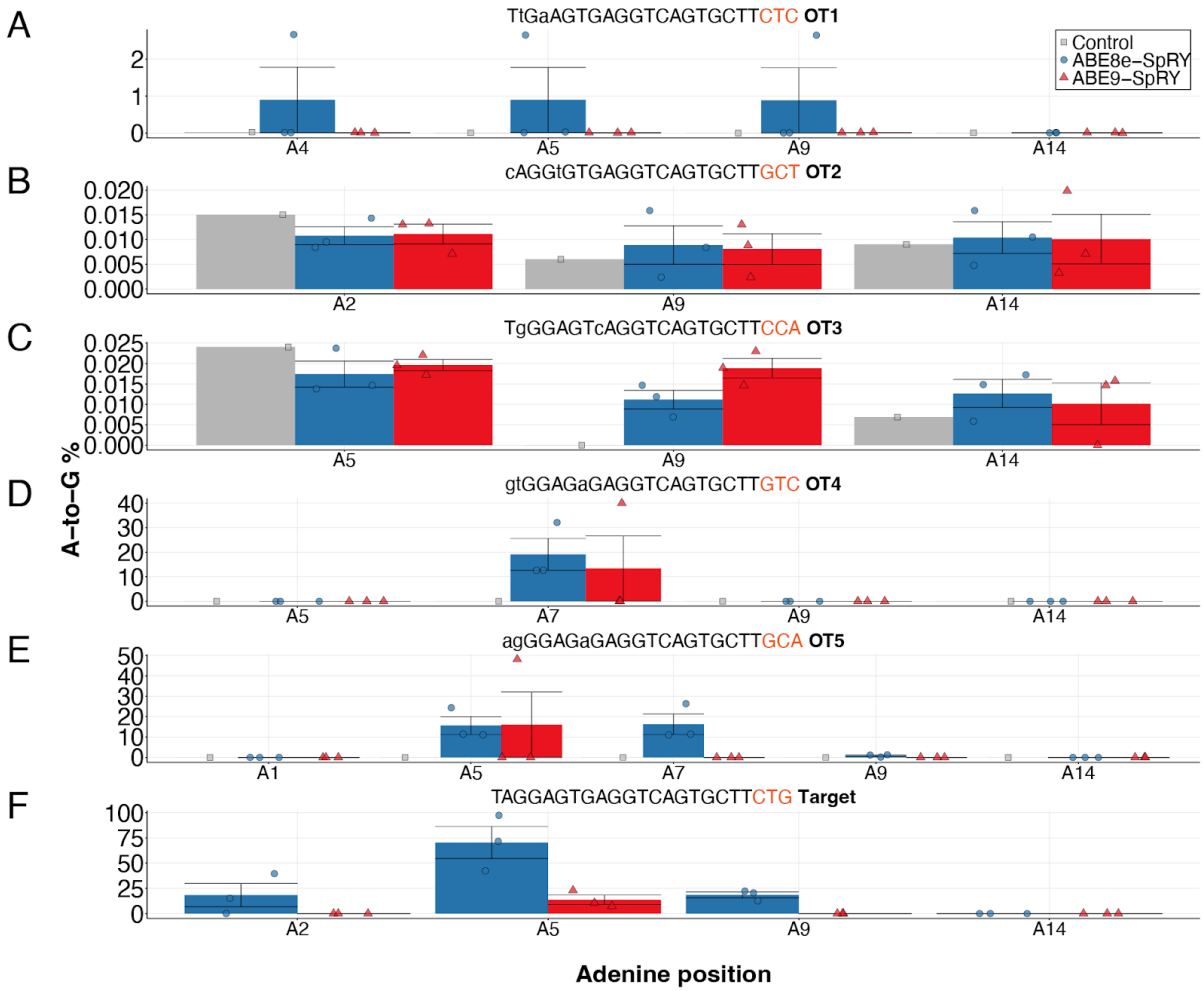

Supplementary Figure 5. ***Tpc2^{L249}*** **off-target analysis. A-E,** A-to-G frequency analysis of the top five predicted off-target site across all adenines within the protospacer sequence. Mismatches compared to the on-target sequence (**F**) are shown by lowercase letters while the PAM sequence is highlighted in orange. **F,** Replotting of the on-target A-to-G editing efficiency for the embryos used for off-target evaluation (Fig. 3C). Error bars represent mean ± s.e.m. and individual data points for three independent biological replicates are shown.

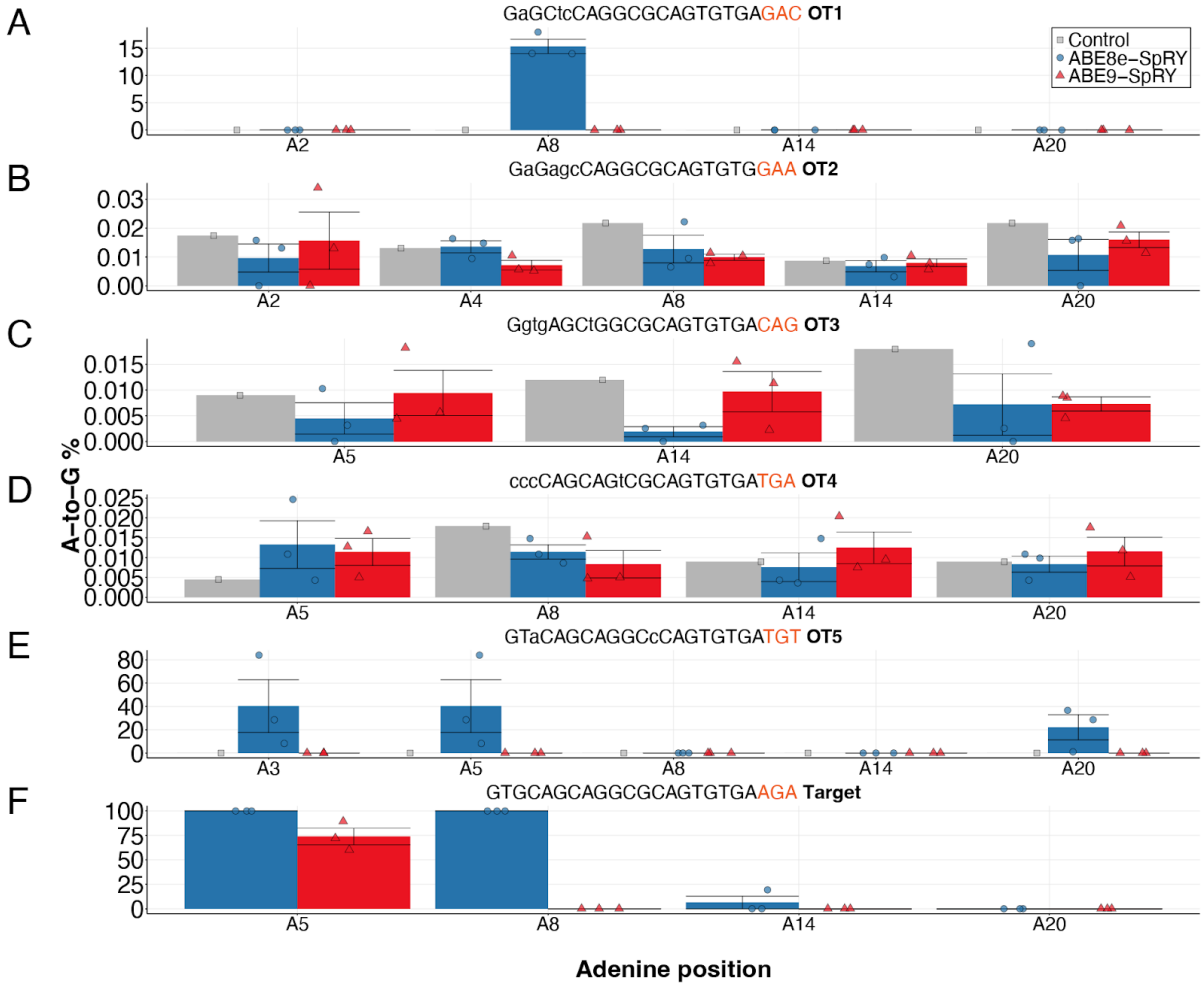

Supplementary Figure 6. ***Trpm4^{L903}*** **off-target analysis. A-E,** A-to-G frequency analysis of the top five predicted off-target site across all adenines within the protospacer sequence. Mismatches compared to the on-target sequence (**F**) are shown by lowercase letters while the PAM sequence is highlighted in orange. **F,** Replotting of the on-target A-to-G editing efficiency for the embryos used for off-target evaluation (Fig. 3C). Error bars represent mean ± s.e.m. and individual data points for three independent biological replicates are shown.

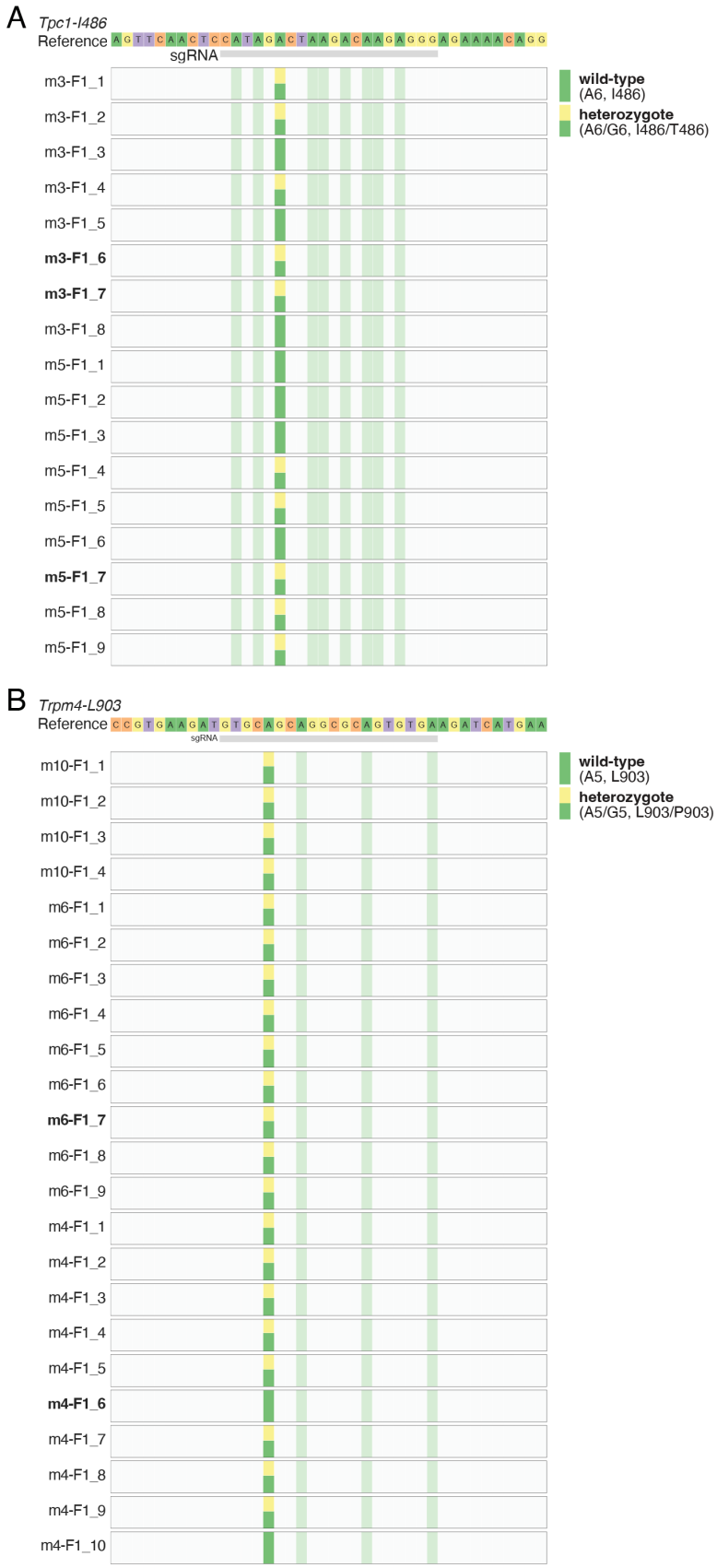

Supplementary Figure 7. **Analysis of F1 transmission from ABE9-SpRY edited sites at the *Tpc1*^{I486} (A) and *Trpm4*^{L903} (B) loci.** Graphs show the base composition in Crispresso2 plots of NGS analysis, highlighting, in colour, any modifications in edited adult mice from ear biopsies compared to the reference sequence 10 bp downstream and upstream of the sgRNA target site. The vertical size corresponds to the frequency of the modification. A total for 17 (**A**) and 21 (**B**), adult mice were analysed to identify heterozygous carriers of the *Tpc1*^{I486T} and *Trpm4*^{L903P}, respectively.

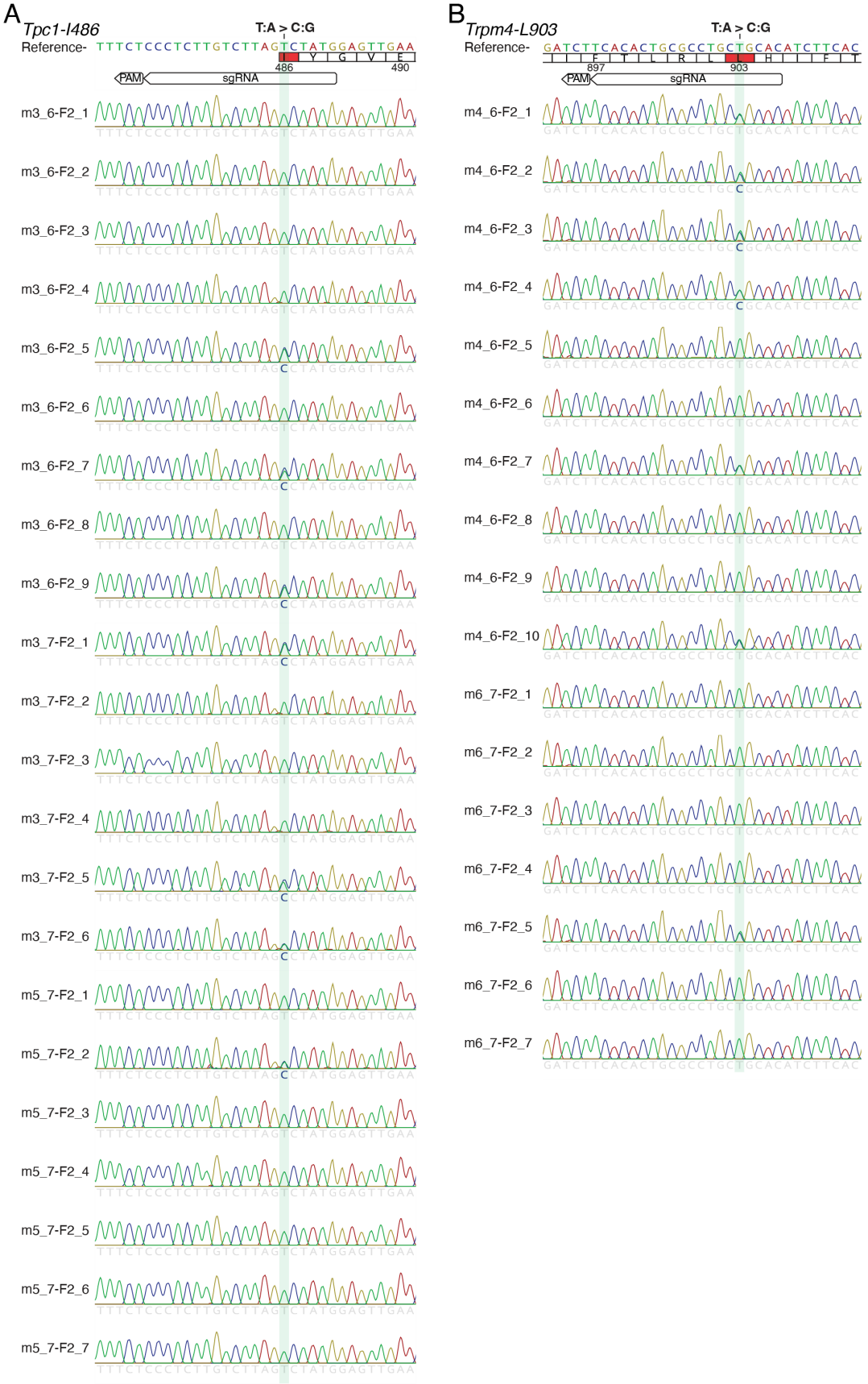

Supplementary Figure 8. **Analysis of F2 transmission from ABE9-SpRY edited sites at the *Tpc1*^{I486} (A) and *Tpc2*^{L249} (B) loci.** Sanger sequencing reads for 22 and 17 F2 mouse ear biopsies were analysed for heterozygous carrier status of the *Tpc1*^{I486T} and *Trpm4*^{L903P} mutations, respectively. Note: for both targets, the sgRNA targets the complementary strand. Green shade highlights the mutated base.